EPRI | ELECTRIC POWER RESEARCH INSTITUTE

Creep-Fatigue Testing and Assessment Guideline

Material Property Data Requirements for Component Assessment

2010 TECHNICAL REPORT

Creep-Fatigue Testing and Assessment Guideline

Material Property Data Requirements for Component Assessment

1019778

Technical Report, December 2010

EPRI Project Manager
B. Dogan

DISCLAIMER OF WARRANTIES AND LIMITATION OF LIABILITIES

THE FOLLOWING ORGANIZATION, UNDER CONTRACT TO EPRI, PREPARED THIS REPORT:

Stuart Holdsworth

NOTE

For further information about EPRI, call the EPRI Customer Assistance Center at 800.313.3774 or e-mail askepri@epri.com.

Acknowledgments

The following organization, under contract to the Electric Power Research Institute (EPRI), prepared this report:

Stuart Holdsworth
Ahornstrasse 11
8600 Dübendorf
Switzerland

Principal Investigator
S. R. Holdsworth

This report describes research sponsored by EPRI.

EPRI thanks Dr. R. Swindemen, Dr. Y. Takahashi, and Dr. A. Scholz for their contribution of data to the creep-fatigue data workbooks and also acknowledges the National Institute for Materials Science, Japan, for permission to use data from its fatigue and creep data sheets.

This publication is a corporate document that should be cited in the literature in the following manner:

Creep-Fatigue Testing and Assessment Guideline: Material Property Data Requirements for Component Assessment. EPRI, Palo Alto, CA: 2010. 1019778.

Abstract

This report reviews material property data requirements for the assessment of defect-free components subject to creep-fatigue loading during service duty. Examples of data input parameters are presented based on an evaluation of information contained in four Electric Power Research Institute (EPRI) creep-fatigue data workbooks compiled for 1CrMoV, 2¼CrMo (Grade 22), 9CrMoVNb (Grade 91), and Grade 316 steels. The background of the creep-fatigue data workbooks is also introduced.

An important step in the assessment of creep-fatigue integrity is the determination of the state of stress and strain at critical locations of the component under evaluation. This requires a knowledge of the external forces and thermal transients experienced by the component during service, as well as representations of the cyclic and creep deformation properties of the materials of construction in terms of model constitutive equations. Options for these are reviewed with examples.

With this information, the state of damage at critical locations can be determined as a function of cycle number, and the material property data required to do this are also reviewed with examples.

The advantages of using properties determined from prior creep deformed or damaged and prior fatigue deformed or damaged materials are explored.

In reviewing the material property data requirements for creep-fatigue assessment, the importance of data pre-assessment and differentiating between creep-fatigue deformation and damage interaction effects, in particular for the 9–11% Cr steels, is also examined.

Keywords

Creep fatigue
Creep-fatigue interaction
Creep deformation
Cyclic deformation
EPRI creep-fatigue data workbooks
Material property data requirements

Contents

List of Figures

List of Tables

1 Introduction

1.1 Background

In 2006, the Electric Power Research Institute (EPRI) convened a group of international experts on creep-fatigue damage interaction to do the following:

- Assess and document current test methods and available data.
- Evaluate analytical methodologies with respect to crack initiation and growth.
- Consider life prediction methodologies for different applications.
- Assess deficiencies that exist in the area of creep-fatigue damage and identify future research and development requirements.

One outcome of this initiative was the compilation of four of EPRI creep-fatigue data workbooks. The concept behind these is introduced in the next section, and details of the current status of the data workbooks are given in Appendix A (which refers to [1–26]). A nomenclature listing is given in Appendix B.

The main driving force behind the generation of the data workbooks was the need to provide a source of materials property data to underpin the model equations on which the creep-fatigue assessment of components could be based. The present report defines material property requirements for component assessment and uses evidence contained in the data workbooks to determine the parameters for model equations that can be used to provide material property input in creep-fatigue assessment procedures.

1.2 EPRI Creep-Fatigue Data Workbooks

The EPRI creep-fatigue data workbooks are based on the concept introduced in reference [1]. This involves the storage of creep-fatigue data on three levels, that is, experimentally determined data reduced to a feasible quantity (Level 1), summary data (Level 2), and assessed data (Level 3), as presented in Appendix A. A brief overview of the tests used to generate the data contained in the data workbooks is given in Section 2.

Data workbooks have been established for four steels, namely, 1CrMoV [2], 2¼CrMo (Grade 22) [3], 9CrMoVNb (Grade 91) [4], and Grade 316 [5].

1.3 Creep-Fatigue Interaction

Critical locations in high-temperature power plant components may be subject to the combined accumulation of cyclic damage arising from strain transients generated during startup and shutdown operation and creep damage arising from primary (directly applied) and secondary (self-equilibrating) stresses during operation.

The development of creep-fatigue damage in most power-plant steels depends on temperature, strain range, strain rate, hold time, and the creep strength and ductility of the material. [8, 27, 28]. In the absence of a significant hold time (and/or at relatively high strain rates), crack initiation and growth are fatigue dominated, even at high application temperatures (see Figure 1-1, panel a). With increasing hold time (and/or decreasing strain rate) at high temperatures, the creep damage condition within the structure becomes increasingly influential, to the limit beyond which crack development becomes fully creep dominated (see Figure 1-1, panel b). At intermediate hold times and strain rates, fatigue cracking interacts with creep damage developing consequentially or

simultaneously, resulting in accelerated crack propagation (see Figure 1-1, panels c and d). The extent of any interaction increases with decreasing creep ductility [27]. The interaction of fatigue and creep is not limited to the accumulation of damage. Deformation interactions are also influential, and they are a dominant influence for some alloys under certain conditions [29].

1.4 Creep-Fatigue Assessment Procedures

Various published and in-house procedures are adopted to assess the integrity of defect-free components subject to creep-fatigue loading, but in general, they require essentially the same material property input data (see Figure 1-2) [30–33]. Other approaches are available (for example, [34–36]), but not so widely adopted. An important step in any procedure is a determination of the state of stresses and strains at the critical location(s) in the component. This requires a knowledge of the external forces and thermal transients experienced by the component during service and representations of cyclic and creep deformation properties of the material(s) of construction in terms of model constitutive equations (see Section 3). The magnitudes of stresses and strains generated during thermal transients depend largely on the physical properties of the material at the critical location, such as coefficient of expansion, thermal conductivity, and elastic modulus. Irrespective of whether the local stress-strain state is determined by approximate analytical solutions or finite element analysis (FEA), the constitutive model options are generally the same.

With this information, fatigue and creep damage fractions can be determined (Section 4). Fatigue damage fraction is commonly determined in terms of cycle number fraction, $N/N_i(\Delta\varepsilon)$, where $N_i(\Delta\varepsilon)$ could be the low-cycle fatigue (LCF) or the cyclic/hold creep-fatigue test crack initiation endurance. The method of determination of creep damage fraction can depend on whether it is accumulated due to primary (directly applied) or secondary (self-equilibrating) loading. Regardless of the approach adopted, the material properties required are derived from the results of creep-rupture tests (Section 2).

With a knowledge of the fatigue and creep damage fractions accumulated per cycle at the component critical location, it is then possible to determine lifetime, for example, by means of a damage summation diagram construction (see Figure 1-2). Typically, such diagrams are constructed from the results of cyclic/hold (LCF with hold time) creep-fatigue tests or thermo-mechanical fatigue (TMF) tests and indicate the extent of any creep-fatigue interaction of the specific material (see Figure 1-1) [29].

It is important to recognize that there is not a unique set of model equations that represent the material property data input requirements of all creep-fatigue assessment procedures, analysis, and material types. However, the test data forming the basis of the required material model representations generally originate from the same experiment types (Section 2). The material property data requirements for the defect-free creep-fatigue assessment of high-temperature components are reviewed in the present report and summarized in Section 5.

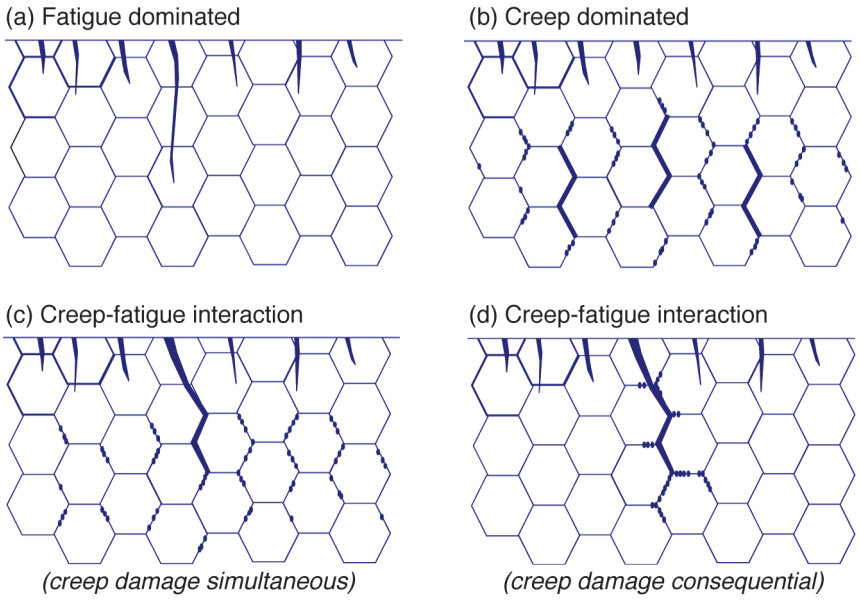

Figure 1-1
Creep-fatigue cracking mechanisms [24]: (a) fatigue dominated, (b) creep dominated, (c) creep-fatigue interaction (due to simultaneous creep damage accumulation), and (d) creep-fatigue interaction (due to consequential creep damage accumulation)

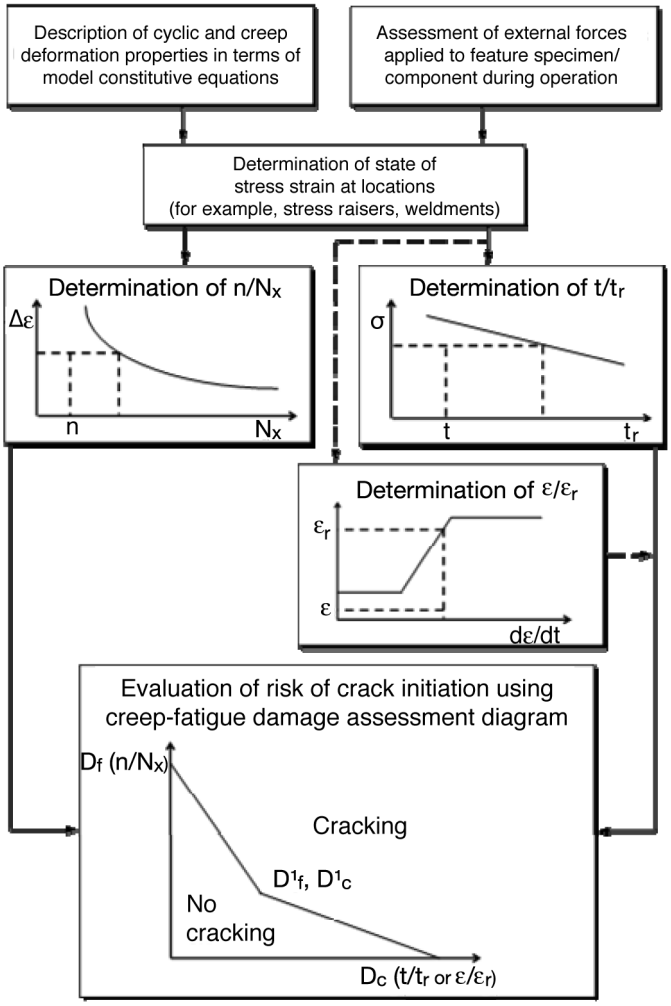

Figure 1-2
Generic flow diagram representing analysis route adopted by a number of defect-free creep-fatigue assessment procedures (for example, [30–33])

2 Sources of Material Property Data

2.1 Overview

The model equations used for determining the stress-strain state (Section 3) and damage condition (Section 4) originate from the results of low-cycle fatigue (without and with hold times) and creep-rupture tests. Section 2 is a general overview of the tests employed, their control and response variables, and the characteristics typically displayed in the steels and alloys employed for power plant applications.

2.2 Low-Cycle Fatigue

LCF tests can be conducted in load or strain control, although typically for the provision of data for power generation purposes, they are conducted in strain control (for example, [37]). The focus in this section is on strain-controlled tests conducted at a constant (usually elevated) temperature.

LCF tests are generally loaded to give crack initiation or failure endurances in the range 100 to less than 100,000 cycles. At elevated temperatures, the influence of creep processes on deformation and damage response is increased by reducing strain rate(s) during strain transients and/or by increasing hold times usually (but not exclusively) at peak strain in tension (for example, see Figure 2-1, panel a). LCF tests generating specimens exhibiting evidence of both fatigue and creep deformation or damage are referred to as creep-fatigue tests [24, 25].

The crack initiation (or failure) endurances from a series of LCF tests with different control $\pm\varepsilon_a$ strain amplitudes provides the basis for an $N_i(\Delta\varepsilon_i)$ model equation, shown in Figure 2-2.

2.2.1 Continuous Cycle Tests

Continuous cycle LCF tests are those without a hold time (that is, with t_h=0). In addition to providing crack initiation or failure endurances, they also provide the basis for model representations of cyclic stress-strain response throughout life (see Figure 2-1).

Typically, metals subject to cyclic plastic deformation harden and/or soften during the course of their life, by an amount depending on the temperature and the total (plastic) strain amplitude (see Figure 2-3). As a generality, cyclic hardening is a result of the generation and interaction of dislocations, whereas softening occurs as a consequence of dynamic recovery of the dislocation substructure. Many austenitic steels such as Grade 316 cyclic harden at high temperature, while exhibiting both hardening and softening during the course of life at lower temperatures (see Figure 2-3, panel a). In contrast, low-alloy and martensitic steels such as 1CrMoV and Grade 91 cyclic soften throughout life at temperatures within their application range (see Figure 2-1, panel b, and Figure 2-3, panel b).

The consequent evolution in mechanical response associated with these microstructural changes can lead to a requirement for evolutionary stress-strain representations for some applications.

2.2.2 Cyclic/Hold Creep-Fatigue Tests

Cyclic/hold (LCF with hold time) tests provide crack initiation endurances that can be used to form the basis of creep-fatigue damage summation diagrams. They also provide important information concerning (1) creep-hardened (or creep-softened) cyclic stress-strain behavior and (2) cyclic-hardened (or cyclic-softened) creep response; for example, see Mazza et al. (2004) [38].

2.3 Creep Rupture

Creep-rupture tests are usually conducted in load control (for example, [39]). The results of such tests provide observations to characterize creep deformation response, time to rupture, and rupture ductility, as shown in Figure 2-4.

Creep-rupture properties are determined from the results of a number of creep tests performed for a range of constant temperature and constant stress (usually constant load) conditions, as shown in Figure 2-5. While there is a large quantity of data on creep rupture (or at least stress rupture), data are most commonly available for test durations of >>100 hours at temperatures in a regime close to the maximum application temperature. For power generation applications, such data are typically collected to form the basis of ≥100,000 hours of creep-rupture strength values. Although this information is also required for creep-fatigue assessment, there is an equally important need for creep-rupture properties associated with higher stresses (shorter rupture durations), ideally at temperatures from $T_{C/t}$ to the maximum application temperature.

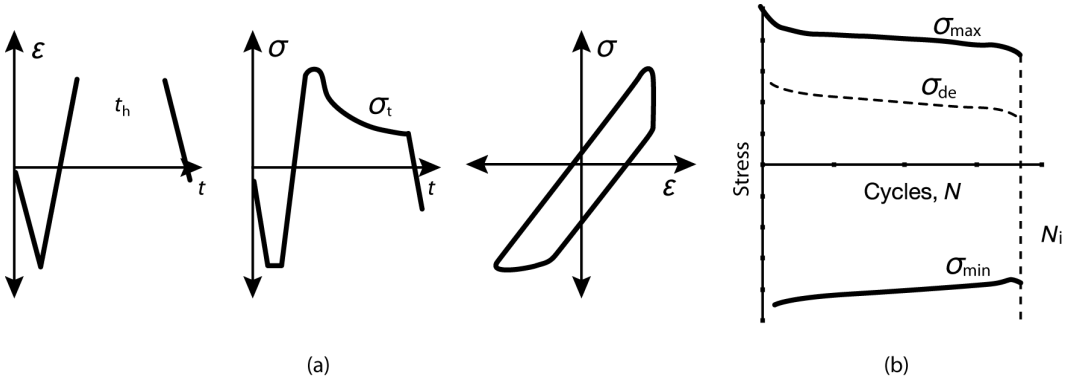

Figure 2-1
Schematic representation of control (ε) and response (σ) variables for LCF test: (a) for a single cycle and (b) for a single test (The diagram shows the case for "with hold time" (cyclic/hold) creep-fatigue tests. For conventional "without hold time" (continuous cycle) tests, t_h is zero, and there is no stress relaxation.)

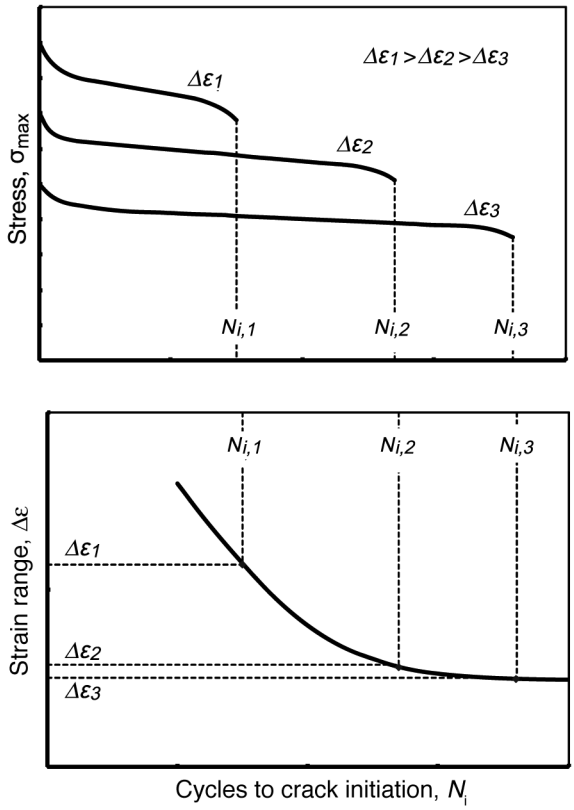

Figure 2-2
Schematic representation of a number of individual LCF tests providing the basis for an $N_i(\Delta\varepsilon)$ endurance model

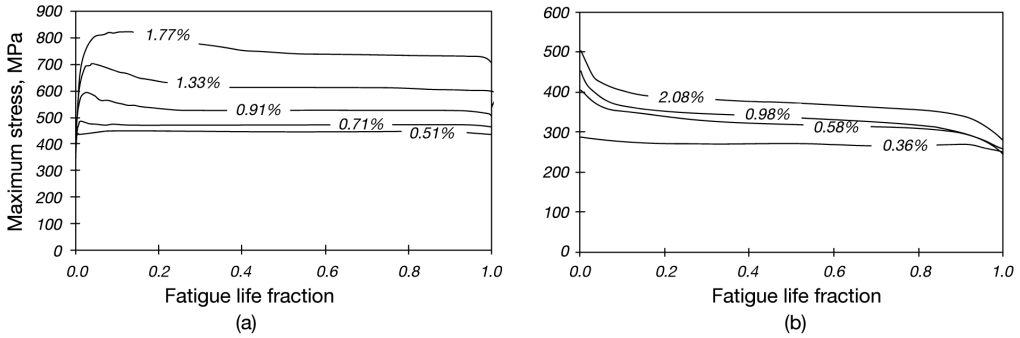

Figure 2-3
Examples of changes in maximum stress with increasing cycle number for (a) a cyclic-hardening steel and (b) a cyclic-softening steel (The data line labels in the two diagrams refer to total strain range.)

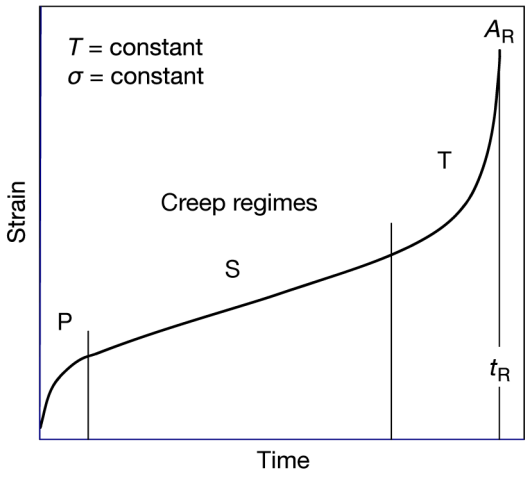

Figure 2-4
Schematic representation of a creep-rupture curve showing primary, secondary, and tertiary deformation regimes

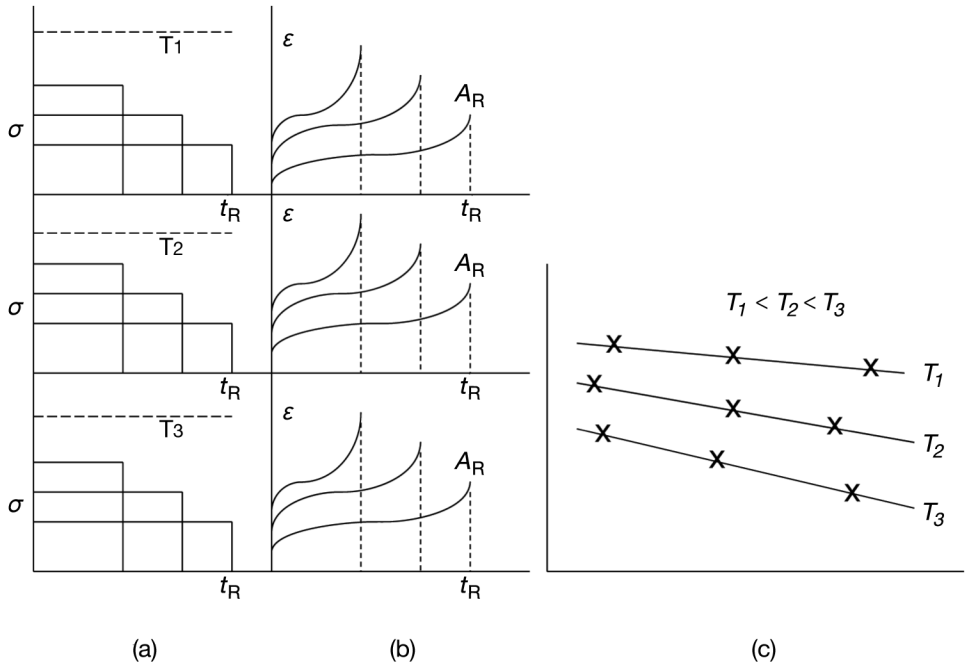

Figure 2-5
Schematic representation of (a) the T,σ dependent-variable conditions for three creep-rupture tests each at three temperatures, (b) the corresponding ε(t) response-variable test records at each temperature, and (c) the resulting t_R(T,σ) data points

3 Model Equations for Deformation Analysis

3.1 Overview

The model equations reviewed in Sections 3 and 4 fall into two categories. In this section, cyclic and creep deformation equations are considered for the determination of stress and strain at critical locations. Fatigue endurance and creep-rupture models that provide a basis for the calculation of damage are reviewed in Section 4. The selection of model equations is not intended to be exhaustive, but simply presented to provide a platform on which to base a concept for the determination of stress-strain state and damage for the purpose of assessing creep-fatigue integrity in high-temperature components.

It is clear from Figure 2-3 that deformation response changes throughout creep-fatigue life, in different ways for different materials. While some cyclic harden, others cyclic soften, or even exhibit both trends before stabilizing. Even for the same material, deformation response characteristics can change with temperature; for example, see Gerland et al. (1997) [40]. The rigorous assessment of stress-strain state throughout life therefore requires the implementation of fully evolutionary deformation models incorporating an internal state variable such as accumulated plastic strain (for example, [38]). In practice, the adoption of such approaches is currently not commonplace, and it is more usual to use deformation models determined using material properties measured at midlife cycles (with the assumption being that on average these reflect the deformation response existing throughout life). The cyclic deformation parameters referred to later in this section are determined from midlife cycle data.

A knowledge of physical properties such as coefficient of expansion (α) and thermal conductivity (k) is important for the determination of stress-strain states arising as a consequence of thermal transients. These are not reviewed in this report, although sources of appropriate values are available [32, 41].

3.2 Elastic Modulus

Despite the fact that elastic modulus is a key parameter for the assessment of stress-strain state in creep-fatigue assessment, there is a tendency for this property to be employed in an overly simplistic way. First, it is important to remember that above the insignificant creep temperature, E becomes strain rate sensitive [42]. Equally important, after the first plastic strain transient in a LCF test, the apparent elastic modulus can reduce or increase significantly [43]. Despite these observations, it is not unusual to adopt data sheet values determined from conventional tensile tests for which the strain rate is not precisely defined or first transient values established during a fatigue test.

For consistency in this report, the E values tabulated in Table 3-1 are used.

Table 3-1
Temperature dependence of elastic modulus

Temperature (°C)	*E* (GPa)			
	1CrMoV	Grade 22	Grade 91	Grade 316
300	192.3	192.9	194.3	177.7
400	183.5	186.5	186.9	169.4
500	170.2	174.9	174.1	160.6
550	161.1	166.2	164.1	156.1
600	150.0	155.0	149.2	151.4
650			128.1	146.7
700				141.8

3.3 Cyclic Deformation

Various model equations are available for the representation of cyclic deformation [17, 44, 45]. These range in complexity from simple bilinear [46] to forms that fully incorporate nonlinear kinematic and isotropic hardening; for example, see Lemaitre and Chaboche (1990) [47]. Many of these can be directly implemented into commonly used FEA codes such as Abaqus [48]. A convenient formulation is that provided by Equation 3-1 [49], and material constants for the Ramberg-Osgood model have been derived for four steels from the information contained in the EPRI creep-fatigue data workbooks (Table 3-2).

$$\Delta\varepsilon = \frac{\Delta\sigma}{E} + \left(\frac{\Delta\sigma}{K}\right)^{1/\beta} \qquad \varepsilon_a = \frac{\sigma_a}{E} + \left(\frac{\sigma_a}{2^{\beta-1}.K}\right)^{1/\beta} \qquad \textbf{Eq. 3-1}$$

A simple version of the Chaboche equation set is given in Equation 3-2. This represents the class of more advanced formulations that are available to fully incorporate nonlinear kinematic and isotropic hardening [45].

$$f = J_2(\boldsymbol{\sigma} - \boldsymbol{X}) = \sigma_o$$
$$\dot{\boldsymbol{X}} = C\dot{\varepsilon}_p\frac{(\boldsymbol{\sigma}-\boldsymbol{X})}{\sigma_o} - \gamma\boldsymbol{X}\dot{\varepsilon}_p + \frac{1}{C}\boldsymbol{X}\dot{C} \qquad \textbf{Eq. 3-2}$$
$$\sigma = \frac{C}{\gamma}(1 - e^{-\gamma\varepsilon_p}) + \boldsymbol{\sigma}_o$$

where symbols in bold represent tensorial quantities.

Cyclic stress-strain observations from the data workbooks are shown for 1CrMoV (in Figure 3-1), Grade 22 (in Figure 3-2), Grade 91 (in Figure 3-3) and Grade 316 (in Figure 3-4). Where available, low-strain-rate and long-hold-time data are also included for comparison with the reference results for a strain rate of 0.001/s. There is a just discernible reduction in the resistance to cyclic plastic deformation as a result of reducing strain rate or the introduction of a 60-minute hold time at peak strain in tension for the low-alloy steels at temperatures in the range 500 to 600°C (see Figures 3-1 and 3-2). However, the reduction is much more notable for the Grade 91 steel, in particular for low-strain-rate cycles (see Figure 3-3). For the Grade 91 steel, reducing the strain rate from 1×10^{-3} to 1×10^{-5}/s is significantly more influential than the introduction of a 60-minute hold time at peak strain in tension.

The effect of reducing strain rate on the cyclic stress-strain response of Grade 316 steel is significantly different from that of low-alloy ferritic and martensitic steels (see Figure 3-4), with austenitic steel exhibiting enhanced flow characteristics at 400 and 500°C and a reduction in the resistance to plastic flow at 600 and 700°C.

Table 3-2
Summary of midlife cycle Ramberg-Osgood constants (determined from data in workbooks)

(a) 1CrMoV

Temp (°C)	$\dot{\varepsilon}$ (s^{-1})	t_h (h)	E (MPa)	K	β
400	0.001	0.0	183,500	1386.0	0.082
500	0.001	0.0	170,200	1062.4	0.062
550	0.001	0.0	161,100	967.5	0.062
600	0.001	0.0	150,000	856.7	0.069

Note: Parameters for Equation 3-1 with $\Delta\varepsilon$ (ε^a) in m/m, and σ in MPa.

(b) Grade 22

Temp (°C)	$\dot{\varepsilon}$ (s^{-1})	t_h (h)	(MPa)	K	β
300	0.001	0.0	192,900	1285.3	0.089
400	0.001	0.0	186,500	1306.7	0.095
500	0.001	0.0	174,900	1092.2	0.089
600	0.001	0.0	155,000	866.8	0.079

Note: Parameters for Equation 3-1 with $\Delta\varepsilon$ (ε^a) in m/m, and σ in MPa.

(c) Grade 91

Temp (°C)	$\dot{\varepsilon}$ (s^{-1})	t_h (h)	E (MPa)	K	β
500	0.001	0.0	174,100	1046.9	0.084
550	0.001	0.0	164,100	1195.1	0.146
600	0.001	0.0	149,200	749.0	0.081
650	0.001	0.0	128,100	523.7	0.079

Note: Parameters for Equation 3-1 with $\Delta\varepsilon$ (ε^a) in m/m, and σ in MPa.

(d) Grade 316

Temp (°C)	$\dot{\varepsilon}$ (s^{-1})	t_h (h)	E (MPa)	K	β
400	0.001	0.0	169,400	3537.9	0.324
500	0.001	0.0	160,600	2334.9	0.213
600	0.001	0.0	151,400	1990.2	0.208
700	0.001	0.0	141,800	1405.3	0.219

Note: Parameters for Equation 3-1 with $\Delta\varepsilon$ (ε^a) in m/m, and σ in MPa.

3.4 Creep Deformation

3.4.1 Insignificant Creep

There is only a need to consider creep if the temperature is high enough for creep effects to be significant. The insignificant creep temperature for a given material is dependent on time. The current recommendation of RCC-MR [32] is that creep effects are insignificant if the total time at any high temperature is less than that which would either (1) give rise to 20% reduction in stress during relaxation at constant strain starting from an initial stress of $1.35.R_{p0.2}$ or (2) accumulate 0.03% creep strain at a constant stress of $1.25.R_{p0.2}$.

Based on these criteria, values have been determined for a number of steels [33]. Indicative values from this source are summarized in Table 3-3.

Table 3-3
Indicative insignificant creep temperatures [33]

Material	$T_{C/10\ h}$ (°C)	$T_{C/100\ h}$ (°C)	$T_{C/1,000\ h}$ (°C)	$T_{C/10,000\ h}$ (°C)	$T_{C/100,000\ h}$ (°C)
Grade 22	450	438	400	377	357
Grade 316	601	567	533	509	482

An alternative solution for determining insignificant creep temperature is to construct a diagram containing $R_{p0.2}$ strength values and $R_{0.2/t/T}$ creep strength values both as a function of temperature. Intersection of the two relations occurs at $T_{C/t}$, the insignificant creep temperature for a specific time.

3.4.2 Creep Strain

There are many model equations available to represent the accumulation of creep strain in the primary, secondary, and tertiary regimes, and the wide spectrum of creep deformation characteristics exhibited by different materials; for example, see Holdsworth (2008) [50]. At the simplest level, and in particular when data are limited, the Norton minimum (secondary) creep rate model is employed [51], that is,

$$\dot{\varepsilon}_{\mathrm{C,min}} = A_{\mathrm{N}} exp(Q_{\mathrm{C}}/RT)\sigma^{n} \qquad \textbf{Eq. 3-3}$$

However, for certain materials under certain conditions, it is necessary to use models that also represent primary and/or tertiary creep deformation, for example,

$$\varepsilon_{\mathrm{C}} = Dexp(Q_{\mathrm{C}}/RT)\sigma^{n}t^{p} \qquad \textbf{Eq. 3-4}$$

$$\varepsilon_{\mathrm{C}} = \varepsilon_{\mathrm{C1}}[1 - exp(-g_1(t/t_{12})^{u})] + \dot{\varepsilon}_{\mathrm{f,min}} + C_{23}(t/t_{23})^{f} \qquad \textbf{Eq. 3-5}$$

The characteristic strain model [52] provides an effective description of primary, secondary, and tertiary creep deformation behavior for metallurgically stable steels when only creep strength and rupture strength data are available.

$$\varepsilon_{\mathrm{C}} = \varepsilon_{\varepsilon}\left(R_{\mathrm{R}/t/T}/R_{\varepsilon/t/T} - 1\right)/\left(R_{\mathrm{R}/t/T}/\sigma - 1\right) \qquad \textbf{Eq. 3-6}$$

Constants for the Norton model (Equation 3-3) have been derived for three steels from the information contained in the data workbooks (Table 3-4). In these examples, the constants have been derived to represent isothermal conditions, and $A_N(\exp(Q_C/RT)$ in Equation 3-3 is replaced by $A_N(T)$.

Table 3-4
Summary of Norton law constants (determined from data in workbooks)

(a) Grade 22

Temp (°C)	$A_N(T)$	n	σ_{max} (MPa)	σ_{min} (MPa)
510	5.523×10^{-22}	7.8	280	145
538	3.962×10^{-22}	8.6	150	40
566	3.130×10^{-19}	7.5	200	110

Note: Parameters for Equation 3-3 with $\dot{\varepsilon}_{C,min}$ in h^{-1}, and σ in MPa.

(b) Grade 91

Temp (°C)	$A_N(T)$	n	σ_{max} (MPa)	σ_{min} (MPa)
500	1.393×10^{-47}	18.1	340	170
600	1.882×10^{-42} 1.788×10^{-22}	17.0 7.7	200 140	140 110
650	7.554×10^{-36} 1.932×10^{-20}	15.3 7.7	130 105	105 55

Note: Parameters for Equation 3-3 with $\dot{\varepsilon}_{C,min}$ in h^{-1}, and σ in MPa.

(c) Grade 316

Temp (°C)	$A_N(T)$	n	σ_{max} (MPa)	σ_{min} (MPa)
600	2.349×10^{-31}	11.0	300	220

Note: Parameters for Equation 3-3 with $\dot{\varepsilon}_{C,min}$ in h^{-1}, and σ in MPa.

There was limited creep deformation data in the version 2 data workbooks (the original focus had been on the collation of LCF and cyclic/hold creep-fatigue test data). This is reflected by the quantity of illustrative information given in Figure 3-5. Although the use of a Norton law representation provides a relatively simple means of modeling creep strain data, its use as defined in Equation 3-3 is complicated by the fact that n varies with temperature and stress (for example, see Table 3-4, part b, and Figure 3-5, panel b).

Unlike the midlife cyclic stress-strain data given in Table 3-2, which reflect that cyclic (and creep) hardening or softening occurs during life (see Figure 2-3), the creep deformation parameters given in Table 3-4 are based on the response of virgin material only to steady stress and temperature. The effect of cyclic deformation on creep properties can only be determined by performing creep tests on material that has been prior cyclic deformed or by analyzing the cyclic stress-relaxation data derived from cyclic/hold creep-fatigue tests (see Figure 2-1). A comparison of the minimum creep strain rates measured during cycle-1 and midlife cycle dwell periods of cyclic/hold creep-fatigue tests for 1CrMoV and Grade 91 steels is shown in Figure 3-6 [29].

The cyclic response characteristics of Grade 91 are very different from those of the low-alloy steels. Grade 91 cyclic softens to a significantly greater extent during the course of fatigue lifetime (cf. a midlife to cycle-1 softening ratio of ~0.6 for Grade 91 with ~0.8 for 1CrMoV steel). In particular, the creep resistance of Grade 91 is more significantly influenced by cyclic deformation than the low-alloy steels. In Figure 3-6, the midlife to cycle-1 strain ratio for Grade 91 is ~100 compared with that of ~50 for 1CrMoV steel.

3.4.3 Stress Relaxation

When creep deformation is accumulated as a consequence of self-equilibrating (strain-controlled) loading, stress relaxation can be modeled using alternative expressions such as those developed by Feltham [53] or Conway [17]:

$$\sigma_t = \sigma_{\text{init}}\left(1 - B"ln(bt + 1)\right) \quad \textbf{Eq. 3-7}$$

$$\sigma_t = \sigma_{\text{init}} exp(-bt^c) \quad \textbf{Eq. 3-8}$$

Additional stress-relaxation model representations are reviewed in Conway et al. (1975) [17].

The parameters for such model equations can be fitted directly to the stress-relaxation profiles observed during the dwell periods of cyclic/hold creep-fatigue tests. In this way, the effect of cyclic hardening or softening on the creep deformation (stress-relaxation) response can if necessary be quantified on a cycle-by-cycle basis.

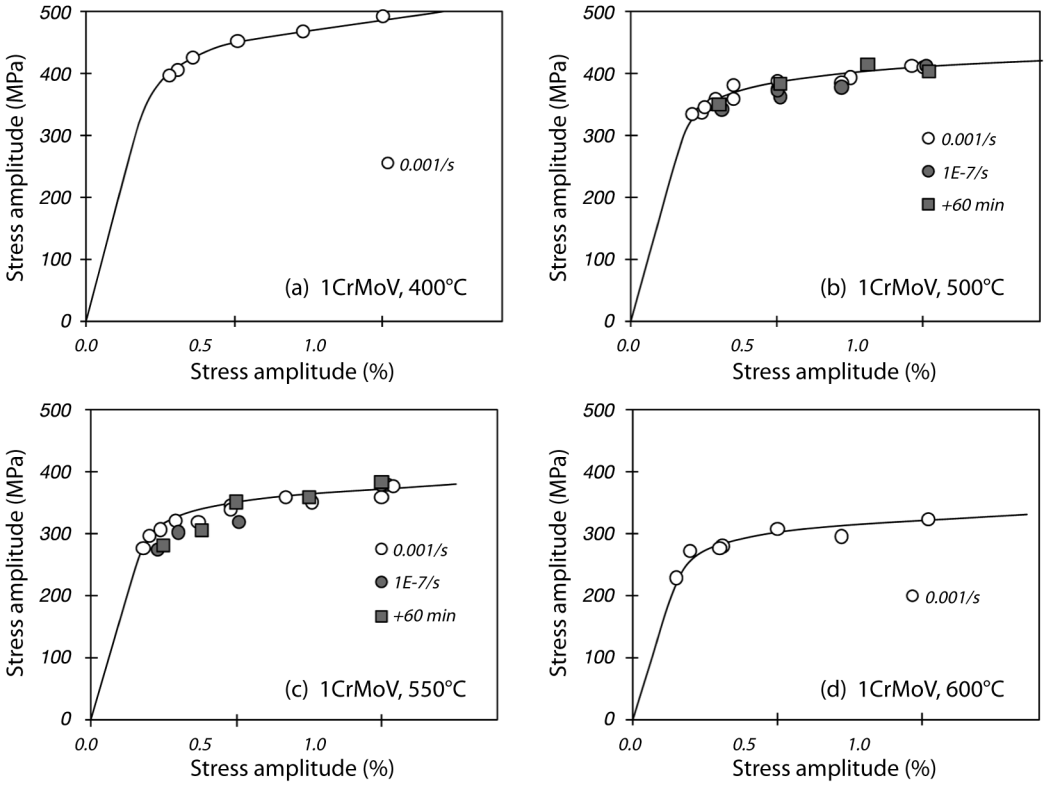

1 MPa = 0.145 ksi
°F = (°C x [9/5]) + 32

Figure 3-1
Midlife cyclic stress-strain properties for 1CrMoV steel extracted from the data workbook [2] (Reference cyclic stress-strain lines are those for a strain rate of 0.001/s defined by the parameters listed in Table 3-2, part a.)

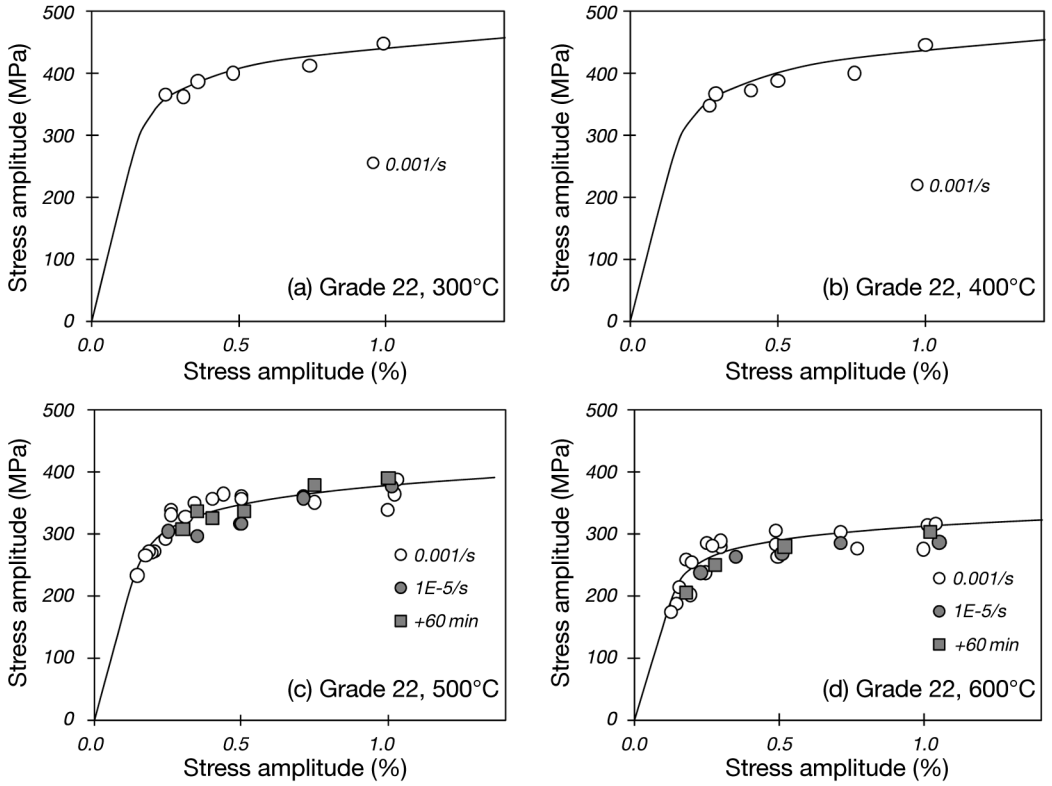

1 MPa = 0.145 ksi
°F = (°C x [9/5]) + 32

Figure 3-2
Midlife cyclic stress-strain properties for Grade 22 steel extracted from the data workbook [3] (Reference cyclic stress-strain lines are those for a strain rate of 0.001/s defined by the parameters listed in Table 3-2, part b.)

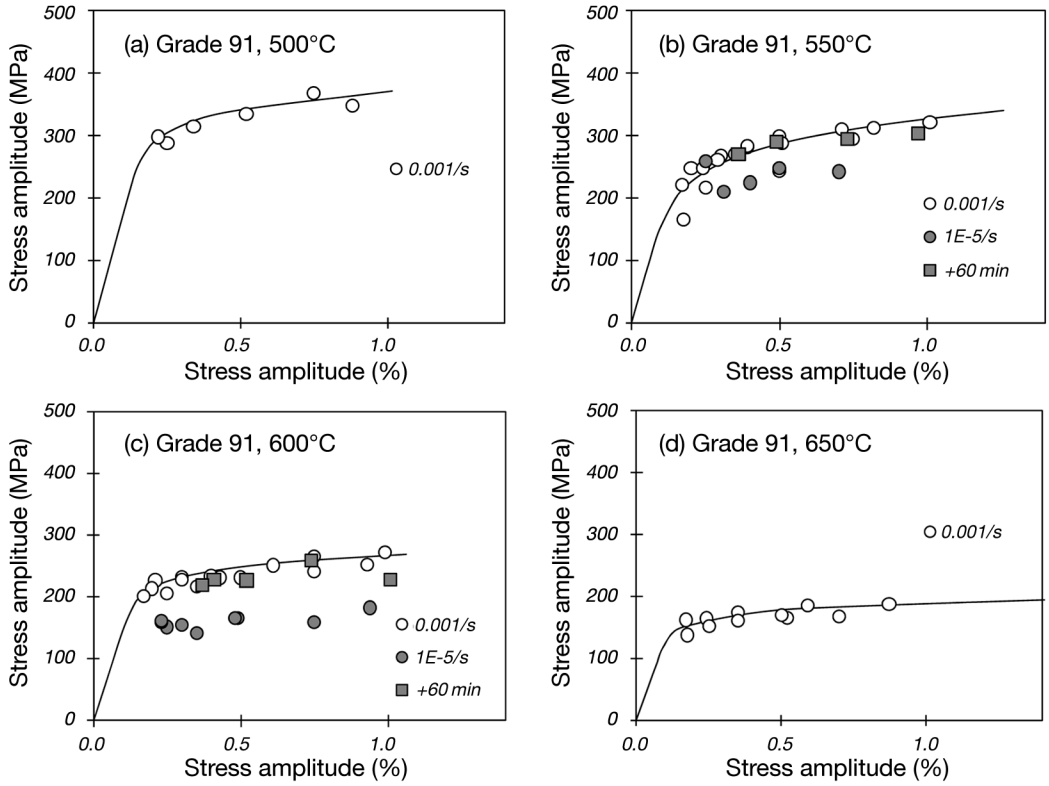

1 MPa = 0.145 ksi
°F = (°C x [9/5]) + 32

Figure 3-3
Midlife cyclic stress-strain properties for Grade 91 steel extracted from the data workbook [4] (Reference cyclic stress-strain lines are those for a strain rate of 0.001/s defined by the parameters listed in Table 3-2, part c.)

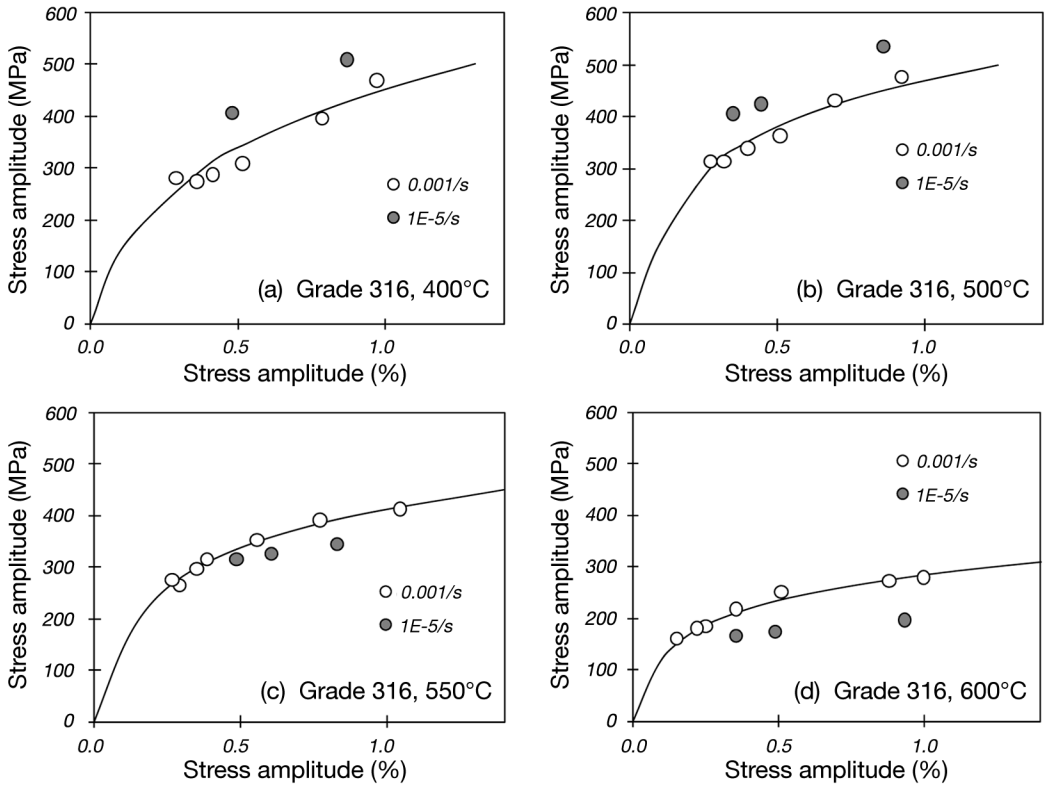

1 MPa = 0.145 ksi
°F = (°C x [9/5]) + 32

Figure 3-4
Midlife cyclic stress-strain properties for Grade 316 steel extracted from the data workbook [5] (Reference cyclic stress-strain lines are those for a strain rate of 0.001/s defined by the parameters listed in Table 3-2, part d.)

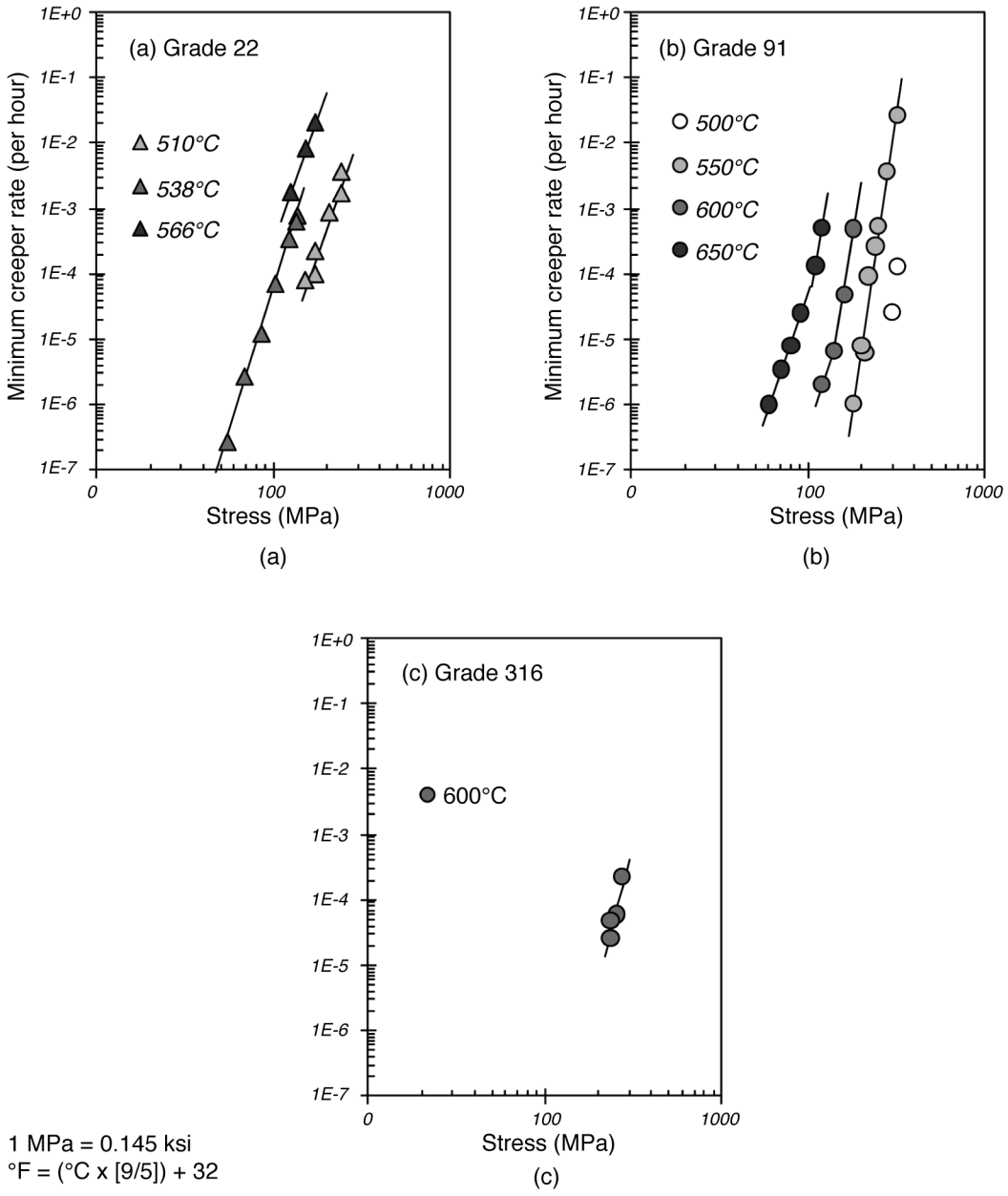

Figure 3-5
Minimum creep rate properties extracted from the data workbook for (a) Grade 22, (b) Grade 91, and (c) Grade 316 (Reference data lines are those defined by the parameters listed in Table 3-4.)

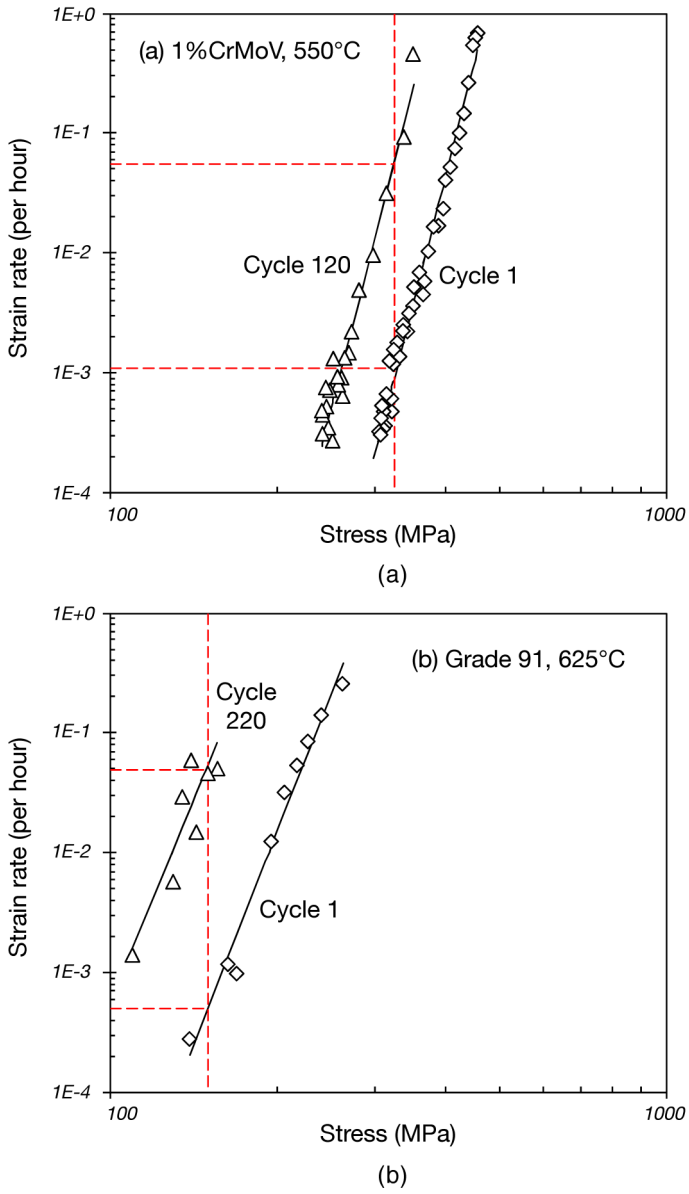

1 MPa = 0.145 ksi
°F = (°C x [9/5]) + 32

Figure 3-6
Comparison of minimum creep strain rates measured during cycle 1 and midlife cycle dwell periods in cyclic/hold creep-fatigue tests on cycle dwell periods in cyclic/hold creep-fatigue tests on(a) 1CrMoV and (b) Grade 91 steels (±0.5%ε_a tests with 30-minute hold time) [29]

4 Model Equations for Damage Assessment

4.1 Overview

In order to predict creep-fatigue crack initiation endurances at component critical locations, it is traditionally necessary first to determine the damage fractions caused by cyclic and steady loading (see Figure 1-2). Fatigue damage fraction is commonly determined in terms of cycle number fraction, that is,

$$d_{\mathrm{F}} = \frac{N}{N_{\mathrm{i}}(\Delta\varepsilon_{\mathrm{t}})} \qquad \textbf{Eq. 4-1}$$

for which a fatigue endurance model is required. Creep-fatigue assessment procedures are broadly differentiated by the way the components of fatigue and creep damage are determined. In general, they fall into two main categories, depending on how the creep damage as a result of secondary (self-equilibrating) loading is calculated, that is, either by time-fraction [30–32] or strain-fraction [33] analysis methods. Time-fraction methods are currently the most widely used to determine d_C, and they are universally adopted to determine creep usage arising from primary (directly applied) loading, that is,

$$d_{\mathrm{C}}^{\mathrm{P}} = \frac{t_{\mathrm{h}}}{t_{\mathrm{R}}^{*}(\sigma^{\mathrm{P}})} \qquad \textbf{Eq. 4-2}$$

A $t_{\mathrm{R}}^{*}(T,\sigma)$ rupture time model is required for the determination of $d_{\mathrm{C}}^{\mathrm{P}}$. Creep damage fraction caused by secondary loading can be determined as a function of time (Equation 4-3) or strain (Equation 4-4), depending on the adopted procedure, that is,

$$d_{\mathrm{C}(t)}^{\mathrm{S}} = \int^{t_{\mathrm{h}}} \frac{dt}{t_{\mathrm{R}(\sigma^{\mathrm{S}})}^{*}} \qquad \textbf{Eq. 4-3}$$

for which a $t_{\mathrm{R}}^{*}(T,\sigma)$ rupture time model is required, and

$$d_{\mathrm{C}(\varepsilon)}^{\mathrm{S}} = \int^{t_{\mathrm{h}}} \frac{\dot{\varepsilon}_{\mathrm{C}}}{A_{\mathrm{R}}^{*}(\dot{\varepsilon}_{\mathrm{C}})} dt \qquad \textbf{Eq. 4-4}$$

for which a rupture ductility model is required, for example, $A_{\mathrm{R}}(\dot{\varepsilon}_{\mathrm{C}})$.

Candidate options for the models required for the determination of fatigue and creep damage fractions are considered in the next section. The list of options presented here is not exhaustive.

4.2 Fatigue Endurance

4.2.1 Model Equations

The Coffin-Manson equation is the most widely used formulation for representing fatigue crack initiation endurance [54], that is,

$$\Delta\varepsilon_t = \Delta\varepsilon_e + \Delta\varepsilon_p = C_e\left(N_i v^{k_e-1}\right)^{-\gamma_e} + C_p\left(N_i v^{k_p-1}\right)^{-\gamma_p} \quad \text{Eq. 4-5}$$

Equation 4-5 is referred to as the frequency modified Coffin-Manson equation, although the model is commonly used without the frequency terms. Constants for the simpler version of the model (without the frequency terms) have been derived for four steels from the information contained in the data workbooks (Table 4-1). This information provides the basis of $N_i(\Delta\varepsilon)$, required for Equation 4-1.

Table 4-1
Summary of Coffin-Manson equation constants (determined from data in the workbooks)

(a) 1CrMoV

Temp (°C)	$\dot{\varepsilon}$ (s^{-1})	t_h (h)	C_e	γ_e	C_p	γ_p
400	0.001	0.0	7.14×10^{-3}	0.346	6.18×10^{-1}	0.618
500	0.001	0.0	6.86×10^{-3}	0.059	6.48×10^{-1}	0.657
550	0.001	0.0	5.88×10^{-3}	0.054	1.42×10^{0}	0.784
600	0.001	0.0	5.24×10^{-3}	0.056	6.24×10^{-1}	0.706

Note: Parameters for Equation 4-5 with $\Delta\varepsilon_t$ in m/m.

(b) Grade 22

Temp (°C)	$\dot{\varepsilon}$ (s^{-1})	t_h (h)	C_e	γ_e	C_p	γ_p
300	0.001	0.0	7.72×10^{-3}	0.057	7.14×10^{-1}	0.621
400	0.001	0.0	1.16×10^{-2}	0.119	6.24×10^{-1}	0.641
500	0.001	0.0	6.74×10^{-3}	0.055	1.32×10^{0}	0.780
600	0.001	0.0	5.58×10^{-3}	0.057	3.22×10^{0}	0.963

Note: Parameters for Equation 4-5 with $\Delta\varepsilon_t$ in m/m.

(c) Grade 91

Temp (°C)	$\dot{\varepsilon}$ (s^{-1})	t_h (h)	C_e	γ_e	C_p	γ_p
500	0.001	0.0	5.80×10^{-3}	0.058	4.10×10^{-1}	0.574
550	0.001	0.0	7.04×10^{-3}	0.098	2.50×10^{-1}	0.514
600	0.001	0.0	4.52×10^{-3}	0.058	6.82×10^{-1}	0.637
650	0.001	0.0	3.29×10^{-3}	0.045	1.17×10^{0}	0.709

Note: Parameters for Equation 4-5 with $\Delta\varepsilon_t$ in m/m.

Table 4-1 (continued)
Summary of Coffin-Manson equation constants (determined from data in the workbooks)

(d) Grade 316

Temp (°C)	$\dot{\varepsilon}$ (s^{-1})	t_h (h)	C_e	γ_e	C_p	γ_p
400	0.001	0.0	1.57×10^{-2}	0.146	1.36×10^{-1}	0.368
500	0.001	0.0	1.19×10^{-2}	0.113	1.97×10^{-1}	0.471
600	0.001	0.0	1.29×10^{-2}	0.106	1.13×10^{-1}	0.415
700	0.001	0.0	1.07×10^{-2}	0.151	2.72×10^{-1}	0.525

Note: Parameters for Equation 4-5 with $\Delta\varepsilon_i$ in m/m.

An alternative $N_i(\Delta\varepsilon)$ formulation is that proposed by Langer [55].

$$\Delta\varepsilon_t = A_L(N_i)^{-\gamma_L} + B_L \qquad \textbf{Eq. 4-6}$$

Other models are reviewed in Conway et al. (1975) [17].

Fatigue damage is typically determined for the maximum temperature in the operating cycle, but it can also be determined for other effective temperatures [56], for example, the TRD temperature [31]:

$$T_{TRD} = T_{min} + 0.75(T_{max} - T_{min}) \qquad \textbf{Eq. 4-7}$$

Crack initiation endurance observations from the data workbooks are shown for 1CrMoV (in Figure 4-1), Grade 22 (in Figure 4-2), Grade 91 (in Figure 4-3), and Grade 316 (in Figure 4-4). Where available, low-strain-rate and long-hold-time data are also included for comparison with the reference results for a strain rate of 0.001/s. Reducing the strain rate or introducing a 60-minute hold time at peak strain in tension is responsible for a significant reduction in the crack initiation endurance for 1CrMoV (see Figure 4-1) and Grade 22 (see Figure 4-2) in the temperature range 500 to 600°C, but appears to be less influential for the Grade 91 steel (see Figure 4-3). Reducing the strain rate in LCF tests on Grade 316 is also responsible for a reduction in crack initiation endurance (see Figure 4-4).

4.2.2 Prior Creep Effects

Evidence to indicate the influence of prior creep on cyclic crack initiation endurance properties for 1CrMoV steel was systematically collected by Shinya et al. (1987) [57]. This information was reevaluated more recently to show that creep may have a beneficial or detrimental influence on the fatigue crack initiation resistance for this steel, depending on the deformation regime and the mechanism of damage development [58]. Prior to the formation of physical creep damage, either as grain boundary cavities or void/matrix decohesion, fatigue crack initiation resistance is enhanced in material that has accumulated primary or secondary creep deformation (see Figure 2-4). The beneficial effect of creep deformation is reversed once physical creep damage is present (see Figure 4-5). The point at which this occurs depends on the stress and the temperature conditions responsible for creep, and the creep ductility of the steel [27]. At higher stresses and/or lower temperatures, significant physical creep damage is generated relatively late in the creep life in the form of voids due to particle/matrix decohesion, and final fracture is transgranular. In these circumstances, fatigue crack initiation resistance continues to be enhanced until late in the creep life as a result of the softening associated with tertiary creep.

At lower stresses, and/or higher temperatures, physical creep damage in the form of grain boundary cavities can occur relatively early in the creep life when the creep ductility is low and later in life when the creep ductility is higher. The development of physical creep damage at the grain boundaries has an increasingly detrimental effect on fatigue crack initiation resistance.

An analytical representation of the prior creep deformed (PCD) functional surface shown in Figure 4-5 enables the determination of $N_i(\Delta\varepsilon_i)^{PC}$ and an alternative formulation to Equation 4-1, that is,

$$d_F^* = \frac{N}{N_i(\Delta\varepsilon_t)^{PC}} \quad \textbf{Eq. 4-8}$$

This type of approach can provide a more effective estimate of fatigue damage fraction, which can be formulated in an evolutionary way [29], but it requires a more extensive material property database than traditional procedures. Nevertheless, it is a potential solution for the future.

4.3 Creep Rupture

Creep damage is commonly determined in terms of a time fraction based on time-to-rupture models [30–32]. However, the use of a strain-based ductility exhaustion creep damage fraction is strongly promoted in the R5 procedure [33], and so both creep-rupture time and ductility models are reviewed in the following sections.

4.3.1 Rupture Time

There are many expressions which can be used to model time to rupture as a function of stress and temperature, many of which are reviewed in Holdsworth (2010) [59]. Typically, they are classified as time-temperature-parameter (TTP) (Equation 4-9 [60]) or algebraic (Equation 4-10 [61]).

$$t_R^* = exp(\{\sum_{k=0}^{n} \beta_k [log(\sigma)]^k\} (T - T_o)^r / \sigma^{-q} + \beta_5) \quad \textbf{Eq. 4-9}$$

$$t_R^* = exp(\beta_0 + \beta_1 log(T) + \beta_2 log(\sigma_o)/T + \beta_3/T + \beta_4 \sigma_o/T) \quad \textbf{Eq. 4-10}$$

TTP models tend to be more flexible in fitting within the range of the data but less stable in extrapolation, whereas algebraic models can be less flexible in data fitting but are more stable in extrapolation. Depending on the values assigned to the parameters, Equation 4-9 is transformed into a number of traditional TTP models [59]. For example, by setting q = 0 and r = 1, the Larson-Miller equation is obtained. Equation 4-10 is specifically referred to as the SM2 model and can effectively represent the stress-rupture characteristics of a number of alloys (for example, see Table 4-2). An alternative formulation is that proposed by Wilshire [62].

$$t_R^* = \frac{1}{u} ln\left(\frac{1}{k}\right) + \frac{1}{u} ln\left(-ln\left(\frac{\sigma}{R_m}\right)\right) + \frac{Q_C}{RT} \quad \textbf{Eq. 4-11}$$

This model equation has the advantage for creep-fatigue assessment applications in that it can be used to represent the data in the high-stress regime in a way that ensures that rupture strength values do not unrealistically exceed the tensile strength of the material. This is particularly useful for creep analyses for creep-fatigue assessment.

Creep-rupture data for the heats of steel contained in the data workbooks are shown for 1CrMoV (in Figure 4-6), Grade 22 (in Figure 4-7), Grade 91 (in Figure 4-9), and Grade 316 (in Figure 4-9). Significant scatter is evident around the trend lines for Grade 22 (see Figure 4-7), as a result of the data workbook containing results for the steel in various product conditions. Creep properties for normalized and tempered Grade 22 are particularly sensitive to ruling section thickness as a consequence of microstructural variations that arise from differences in the air-cooling rate from the normalizing temperature.

Table 4-2
Summary of constants for SM2 creep-rupture model

(a) Model parameters

Material	β_0	β_1	β_2	β_3	β_4
1CrMoV	–1170.94958	341.558868	2525.28711	152326.453	–30.8134823
Grade 22	–263.457916	67.6636124	–6487.19092	76328.2891	–10.6347399
Grade 91	–235.860962	48.6824532	–8609.15137	110872.758	–31.8743629
Grade 316	–672.226172	185.925171	–8250.51465	139204.547	–19.9724884

Note: Parameters for Equation 4-10 with t_R^* in h, T in K, and σ in MPa.

(b) Limits of applicability

Material	T_{max}	T_{min}
1CrMoV	575°C	450°C
Grade 22	600°C	450°C
Grade 91	650°C	500°C
Grade 316	750°C	500°C

4.3.2 Rupture Ductility

Proven procedures for the assessment of rupture ductility, particularly for large multisource, multicast, multitemperature data sets, are still under development. Such data sets can be highly complex, although there are now model representations that can handle such complexity (for example, see Holdsworth (2004) [63]), with the most promising of these currently being the stress-modified ductility equation of Spindler [64]:

$$ln(A_R^*) = min\left[\left\{ln(A_1) + \frac{Q_C}{RT} + n_1 ln\left(\dot{\varepsilon}_{C,av}\right) + m_1 ln(\sigma)\right\}, ln(A)\right] \quad \textbf{Eq. 4-12}$$

Rupture ductility data for the heats of steel contained in the data workbooks are included in Figure 4-6 (1CrMoV), Figure 4-7 (Grade 22), Figure 4-8 (Grade 91), and Figure 4-9 (Grade 316).

4.3.3 Other Approaches

For the future, there are emerging energy-based models for the determination of creep damage fractions [13, 65].

4.3.4 Influence of Prior Cyclic Deformation

Prior cyclic deformation is responsible for cyclic softening in CrMoV steels, which in turn influences the magnitude of the creep strength [66]. The outcome is a reduction in rupture times and an increase in creep strain rates, but with $\dot{\varepsilon}_{C,min} t_R$ maintaining the same constant of proportionality as the virgin steel (see Figure 4-10, panels a and b). The magnitude by which the rupture time is reduced depends on the magnitude of the stress and the consequent rupture mechanism. At stress levels responsible for a ductile transgranular rupture mechanism (arising from void formation due to particle/matrix decohesion), the reduction in rupture time is significant. In contrast, at stress levels responsible for intergranular rupture (arising from grain boundary cavity formation), the reduction in rupture time is relatively small.

The effect of prior cyclic deformation of the rupture ductility of 1CrMoV steel also depends on stress and strain rate (rupture mechanism) [67]. At stresses (and strain rates) associated with lower and upper shelf rupture ductilities, the influence of prior cyclic deformation and the consequent increase in minimum creep rate is small (see Figure 4-10, panels c and d). At stresses (and strain rates) associated with the transition from upper shelf to lower shelf rupture ductilities, the influence of prior cyclic deformation can be responsible for a significant increase in rupture ductility.

In contrast, for Grade 316 steel the effect of prior cyclic deformation on creep is to increase the time to rupture and reduce the strain rate, with the magnitude of the effect appearing to be relatively insensitive to the applied stress [67], as shown in Figure 4-11, panels a and b. Prior cyclic deformation is responsible for an increase in rupture ductility, as shown in Figure 4-11, panels c and d.

Analytical representations of the data given in Figure 4-10, panels a and d, and Figure 4-11, panels a and d, enable the determination of $t_R(\sigma)^{PF}$, $A_R(\dot{\varepsilon}_C)^{PF}$, and alternative formulations to Equations 4-2, 4-3, and 4-4, that is,

Eq. 4-13

$$d^*_{C(t)} = \int^{t_h} \frac{dt}{t^*_R(\sigma)^{PF}}$$

for which a prior fatigue deformed (PFD) rupture time model is required, and

Eq. 4-14

$$d^*_{C(\varepsilon)} = \int^{t_h} \frac{\dot{\varepsilon}_C}{A^*_R(\dot{\varepsilon}_C)^{PF}} dt$$

for which a PFD rupture ductility model is required.

The use of such models can provide a more effective estimate of creep damage fraction, which can be formulated in an evolutionary way [29], but requires a more extensive material property database than traditional approaches. It is therefore a potential solution for the future.

4.4 Damage Summation

The ways in which creep and fatigue damage can be summed are conveniently illustrated with reference to possible crack initiation locus options in a creep-fatigue damage summation diagram (see Figure 4-12). Bilinear damage loci, as used in the calculations in References 30 and 32, can be modeled using the following equations:

$$D_F = 1 - D_C.(1 - D'_F)/D'_C \quad \text{for } D_C < D'_C$$
$$D_F = (1 - D_C).D'_F/(1 - D'_C) \quad \text{for } D_C > D'_C \qquad \textbf{Eq. 4-15}$$

where D'_F,D'_C define the intersection coordinates [68]. For linear damage accumulation, as in the calculations in References 31 and 33, D'_F,D'_C = 0.5. Alternatives are the L-shaped locus adopted in Bestwick and Clayton (1985) [69] and more recently the quadratic locus that is said to represent the theoretical lower bound [70]. Apart from the theoretically based quadratic representation, other damage summation options are determined on the basis of experimental observations from low-strain-rate LCF, cyclic/hold, or service-cycle TMF tests [26, 71].

In Equation 4-15,

$$D_F = \sum_j N_j d_{F,j} \qquad \textbf{Eq. 4-16}$$

$$D_C = \sum_j N_j d^P_{C,j} + \sum_j N_j d^S_{C,j} \qquad \textbf{Eq. 4-17}$$

where j is the number of service-cycle types, and options for d_F and d_C are considered earlier in this section.

Some analysts account for creep damage caused by secondary loading as part of the fatigue damage fraction calculation by using $N_i(\Delta\varepsilon_t, t_h)$ endurance models based on observations from cyclic/hold creep-fatigue tests in Equation 4-16 [72, 73]. In such circumstances, creep damage fraction is estimated only using the first term in Equation 4-17. It is therefore important to recognize that the damage summation locus depends not only on material and temperature but also on the analysis procedure employed to determine the stress-strain state and to determine the fatigue and creep damage [29]. It should therefore not be assumed without verification that the damage summation diagram given for a specific material (see Figure 4-13) is appropriate for any other creep-fatigue assessment procedure

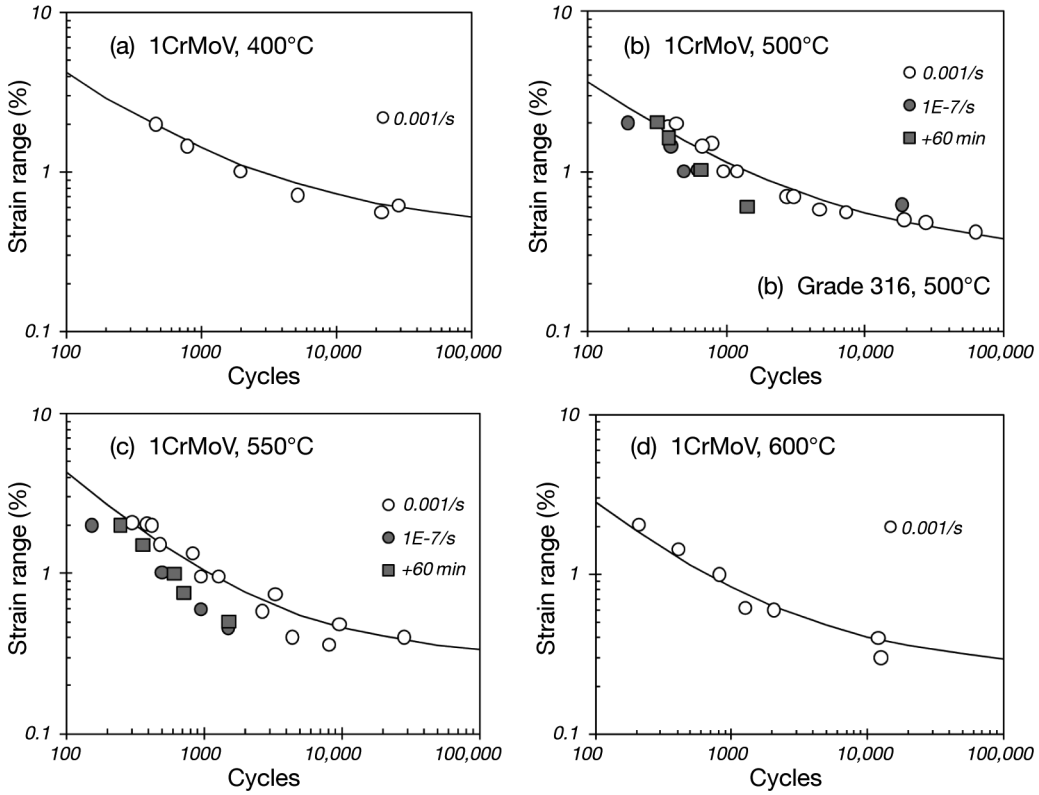

°F = (°C x [9/5]) + 32

Figure 4-1
Crack initiation endurance properties for 1CrMoV steel extracted from the data workbook [2] (Reference LCF lines are those defined by parameters in Table 4-1, part a.)

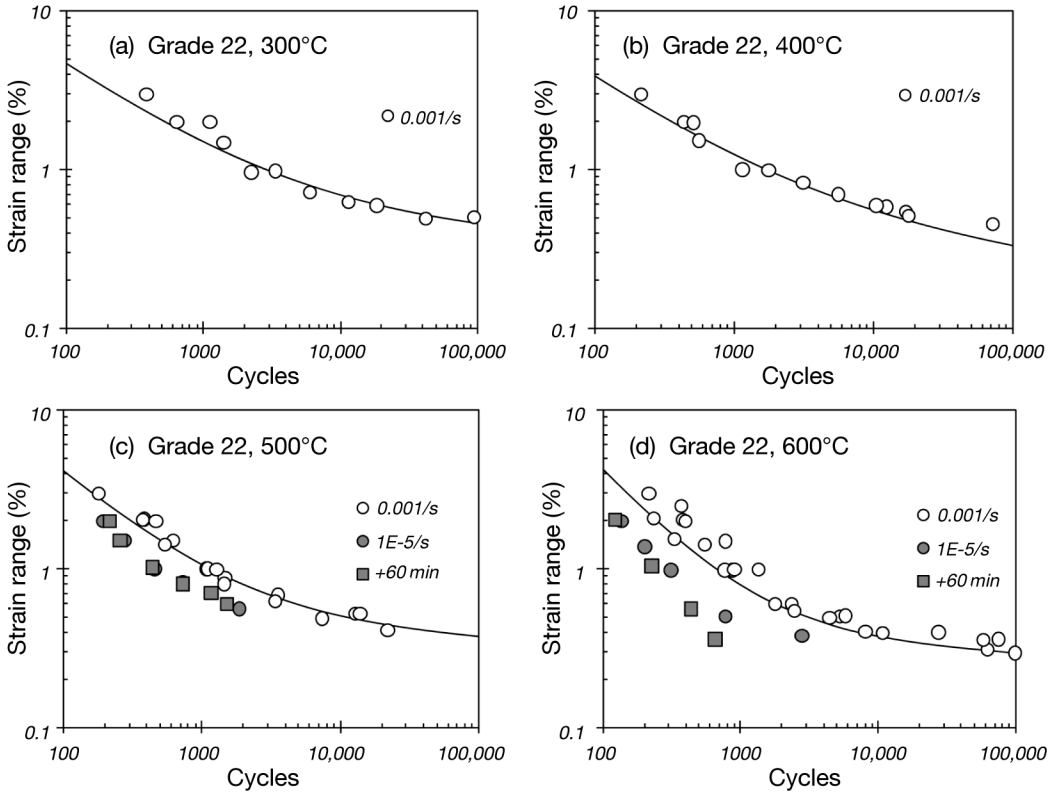

°F = (°C x [9/5]) + 32

Figure 4-2
Crack initiation endurance properties for Grade 22 steel extracted from the data workbook [3] (Reference LCF lines are those defined by parameters in Table 4-1, part b.)

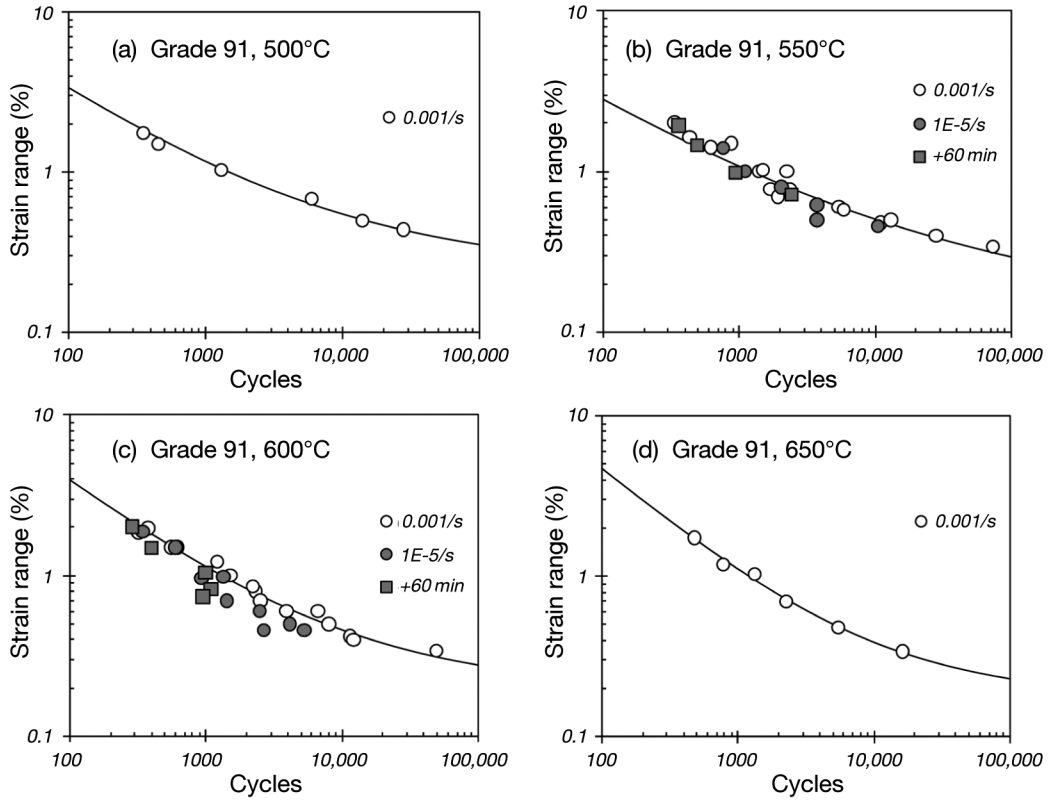

°F = (°C x [9/5]) + 32

Figure 4-3
Crack initiation endurance properties for Grade 91 steel extracted from the data workbook [4] (Reference LCF lines are those defined by parameters in Table 4-1, part c.)

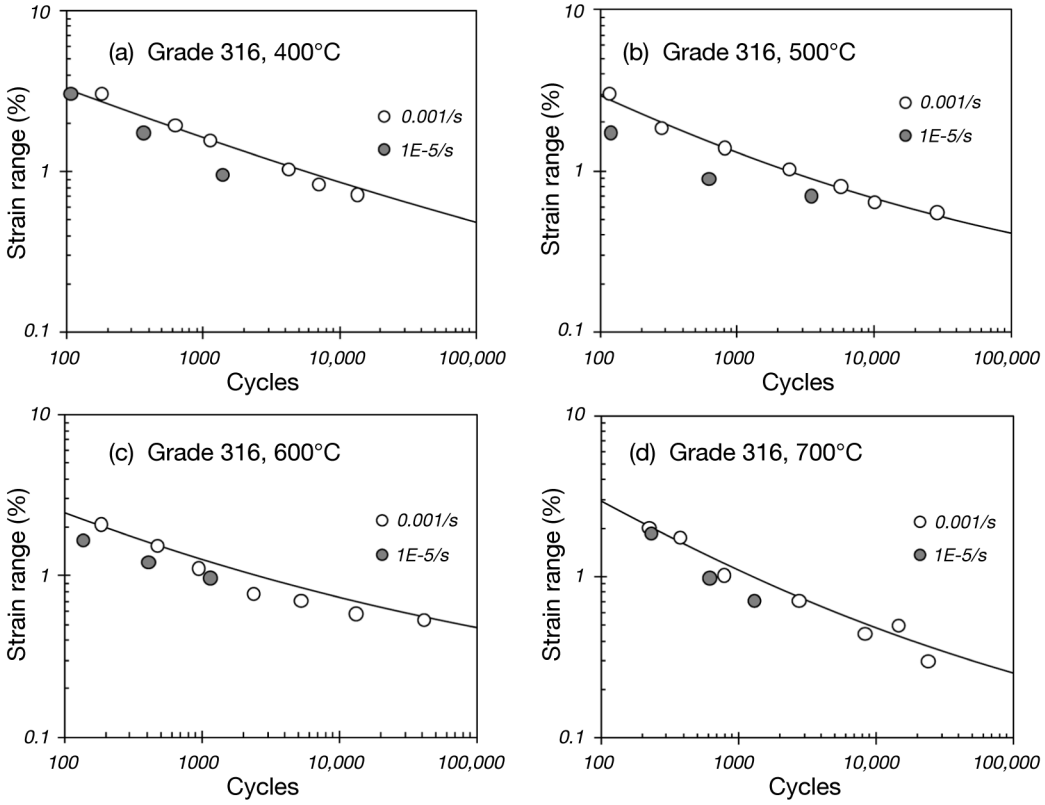

°F = (°C x [9/5]) + 32

Figure 4-4
Crack initiation endurance properties for Grade 316 steel extracted from the data workbook [5] (Reference LCF lines are those defined by parameters in Table 4-1, part d.)

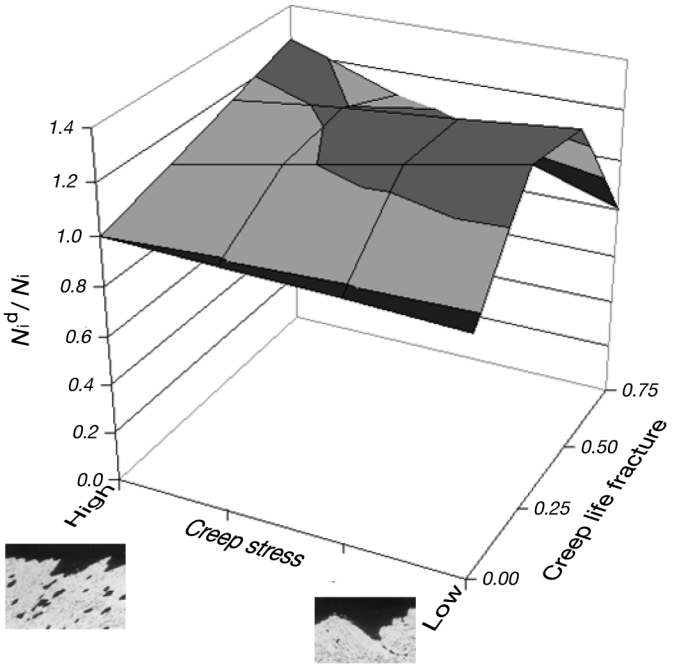

Figure 4-5
Influence of stress responsible for prior creep condition on fatigue crack initiation endurance [58] (In the terminology of this report, the N_i^d/N_i ratio adopted in Binda et al. (2008) [58] is $N_i(\Delta\varepsilon_t)^c/N_i(\Delta\varepsilon_t)$; see Equation 4-8.)

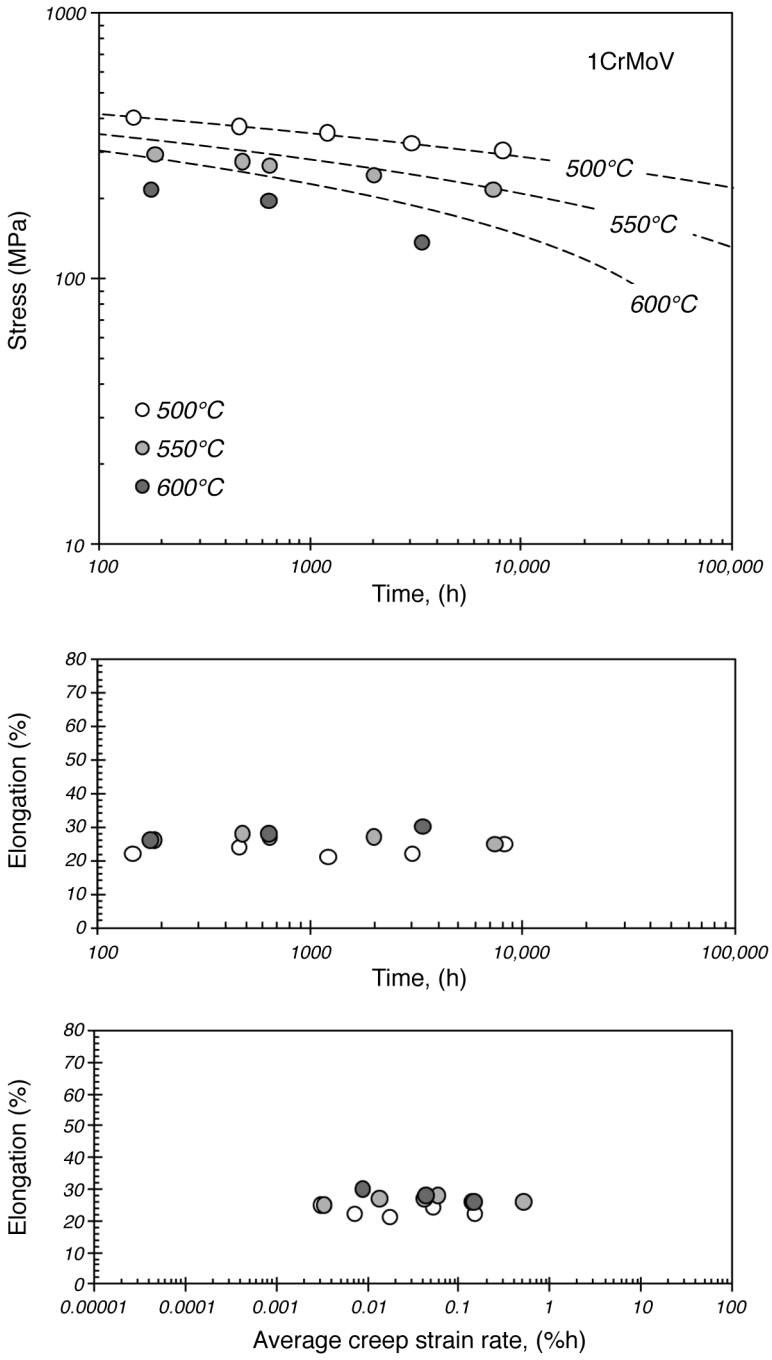

1 MPa = 0.145 ksi
°F = (°C x [9/5]) + 32

Figure 4-6
Summary of creep-rupture strength and ductility values for heats of 1CrMoV steels contained in the data workbook [2] (Reference lines are those defined by parameters in Table 4-2.)

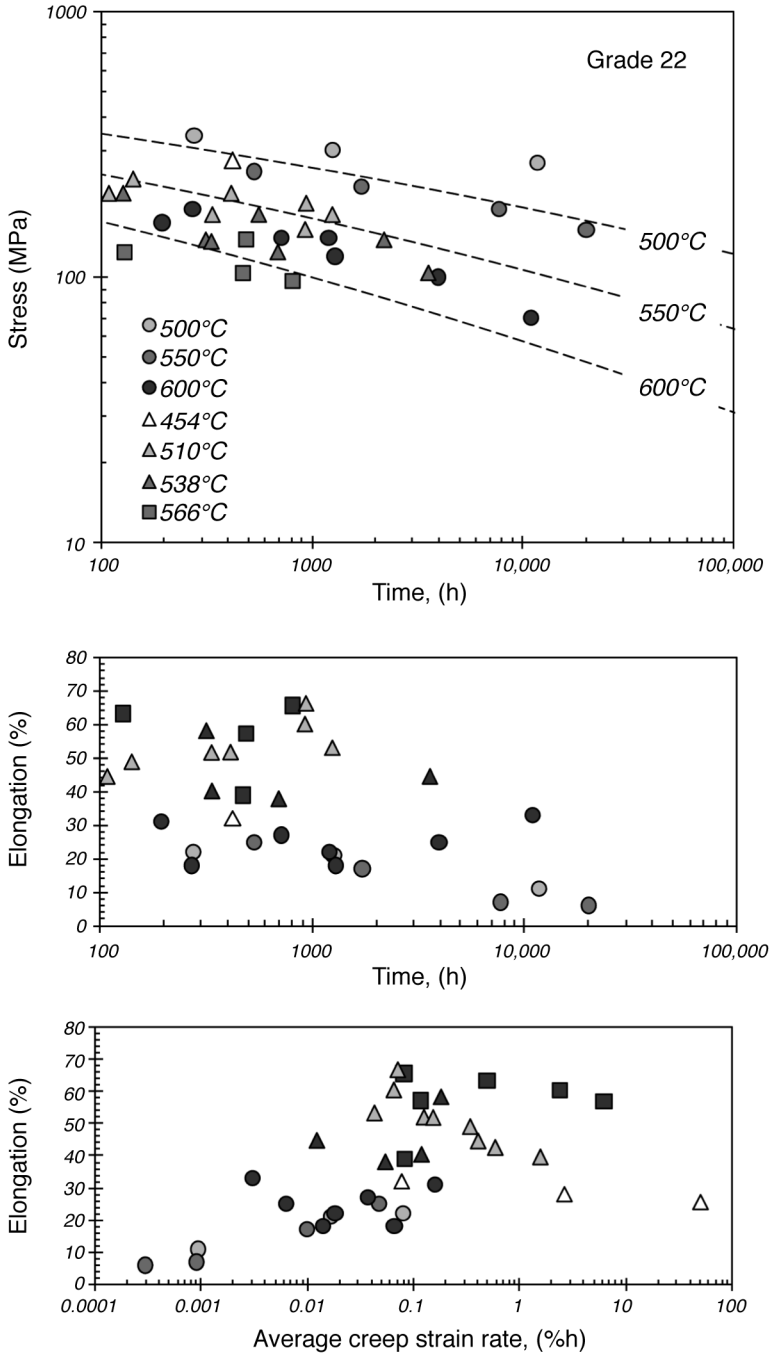

1 MPa = 0.145 ksi
°F = (°C x [9/5]) + 32

Figure 4-7
Summary of creep-rupture strength and ductility values for heats of Grade 22 steels contained in the data workbook [3] (Reference lines are those defined by parameters in Table 4-2.)

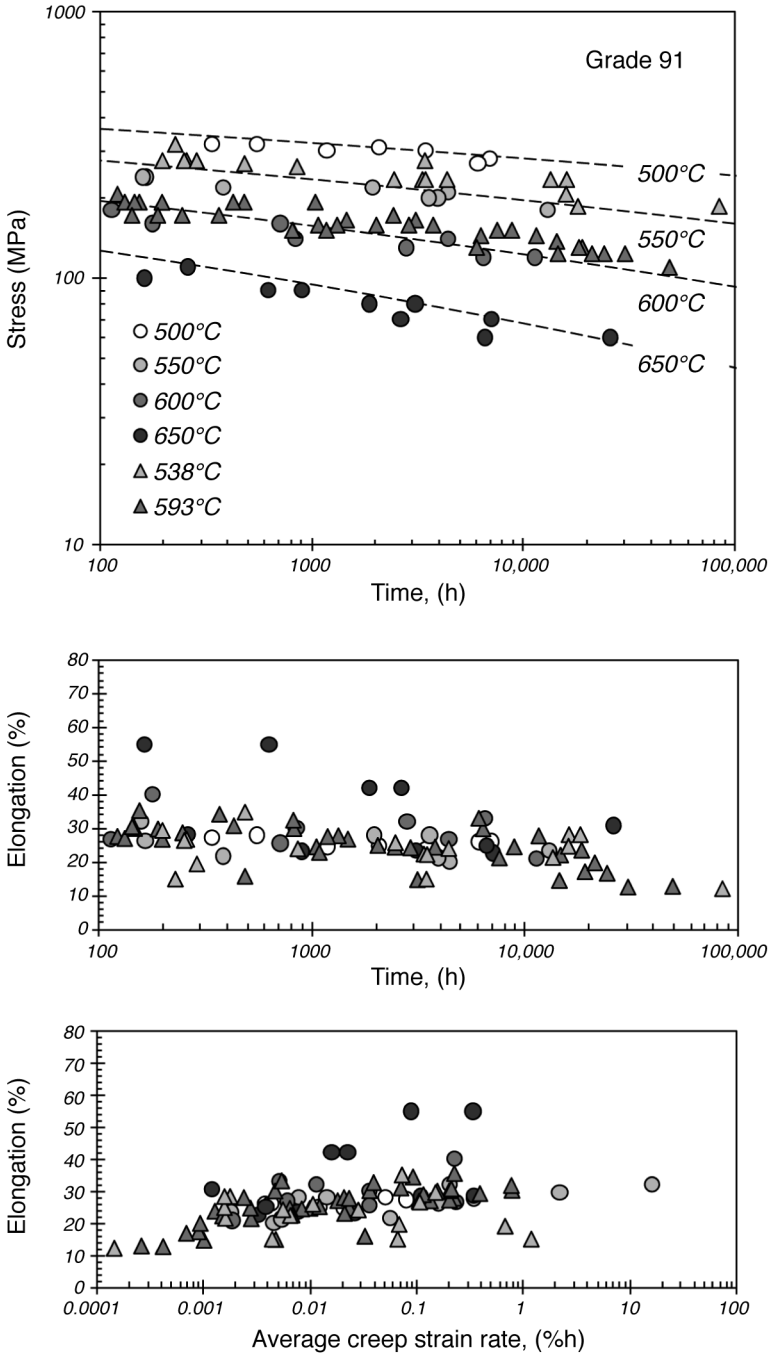

1 MPa = 0.145 ksi
°F = (°C x [9/5]) + 32

Figure 4-8
Summary of creep-rupture strength and ductility values for heats of Grade 91 steels contained in the data workbook [4] (Reference lines are those defined by parameters in Table 4-2.)

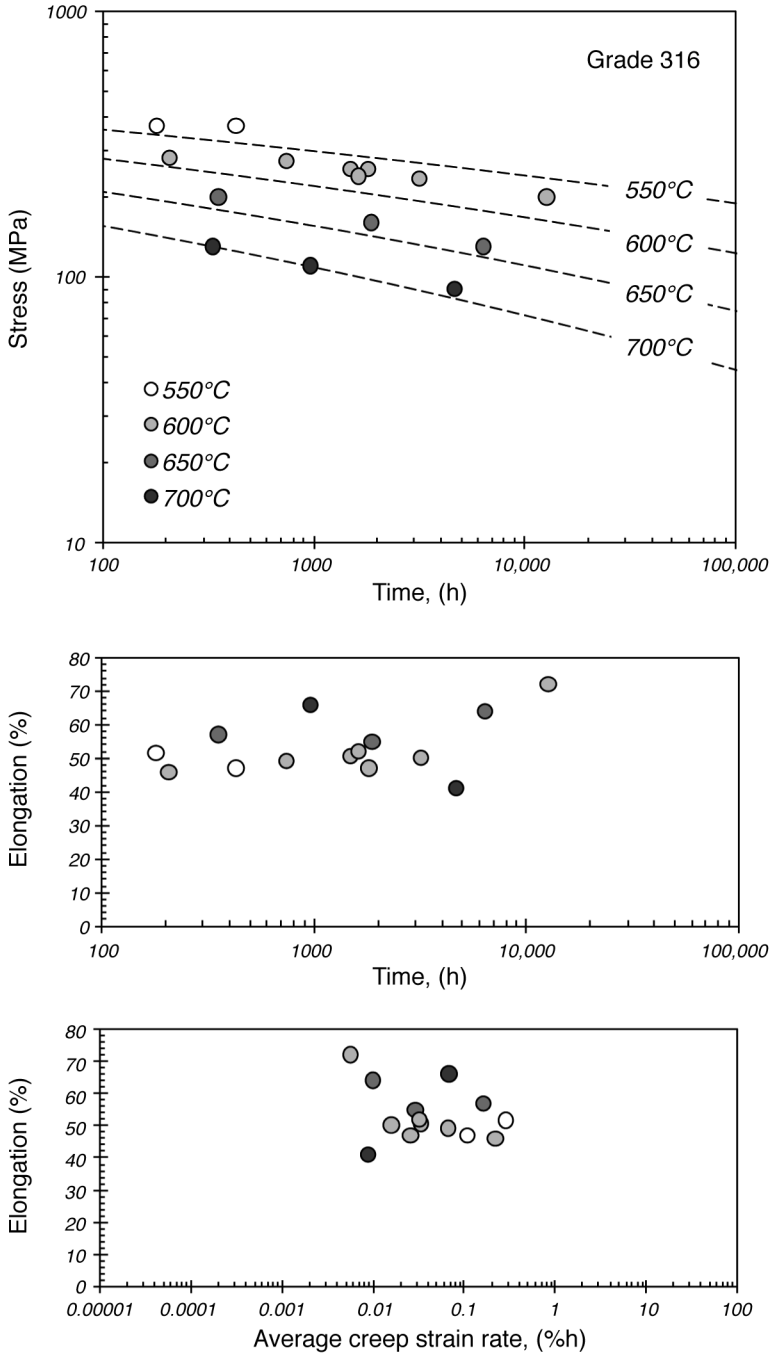

1 MPa = 0.145 ksi
°F = (°C x [9/5]) + 32

Figure 4-9
Summary of creep-rupture strength and ductility values for heats of Grade 316 steels contained in the data workbook [5] (Reference lines are those defined by parameters in Table 4-2.)

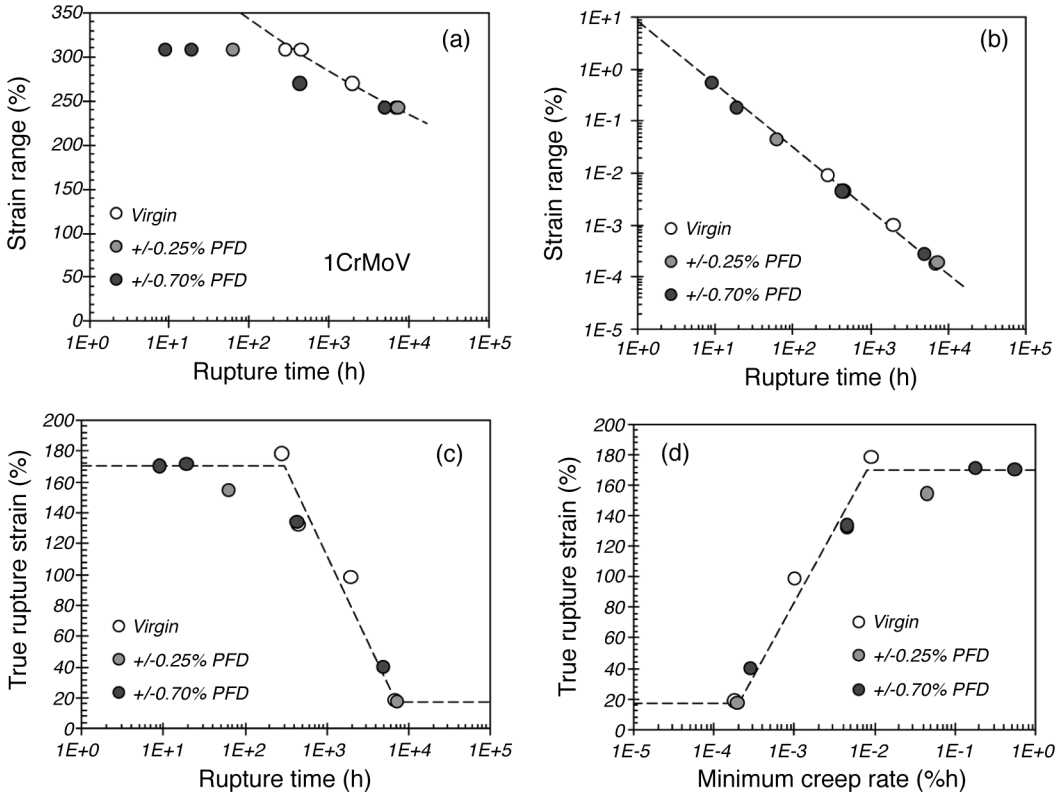

1 MPa = 0.145 ksi

Figure 4-10
Influence of prior fatigue deformation on the creep-rupture properties of 1CrMoV steel [67]

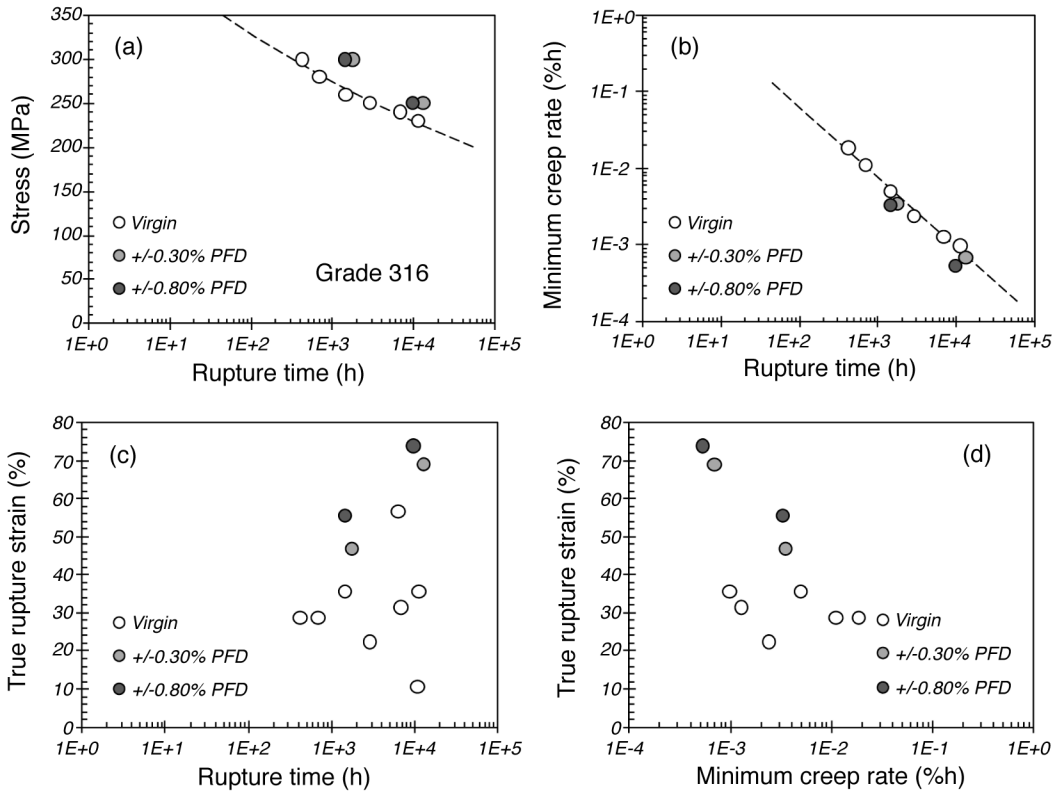

1 MPa = 0.145 ksi

Figure 4-11
Influence of prior fatigue deformation on the creep-rupture properties of Grade 316 [67]

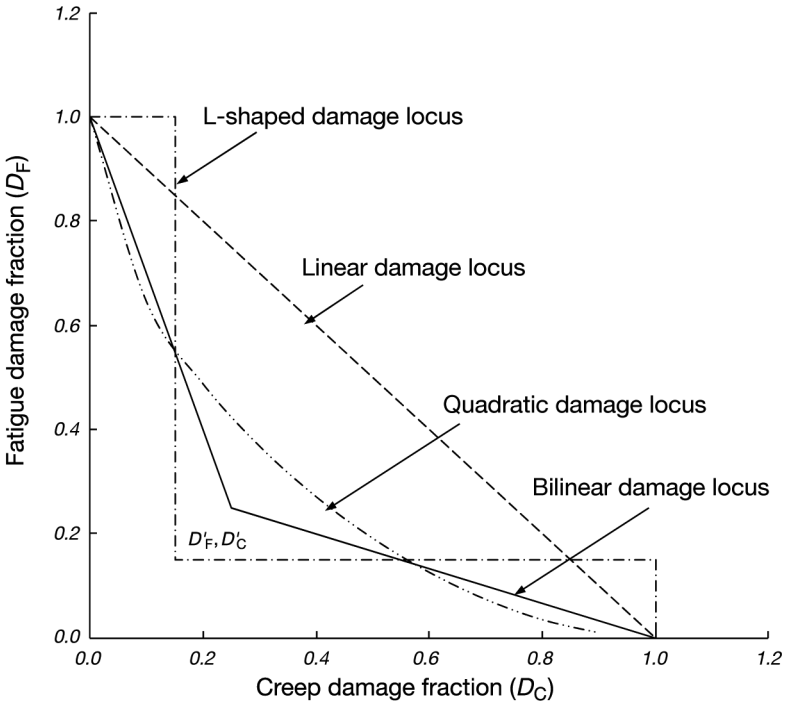

Figure 4-12
Crack initiation locus options in a creep-fatigue damage summation diagram

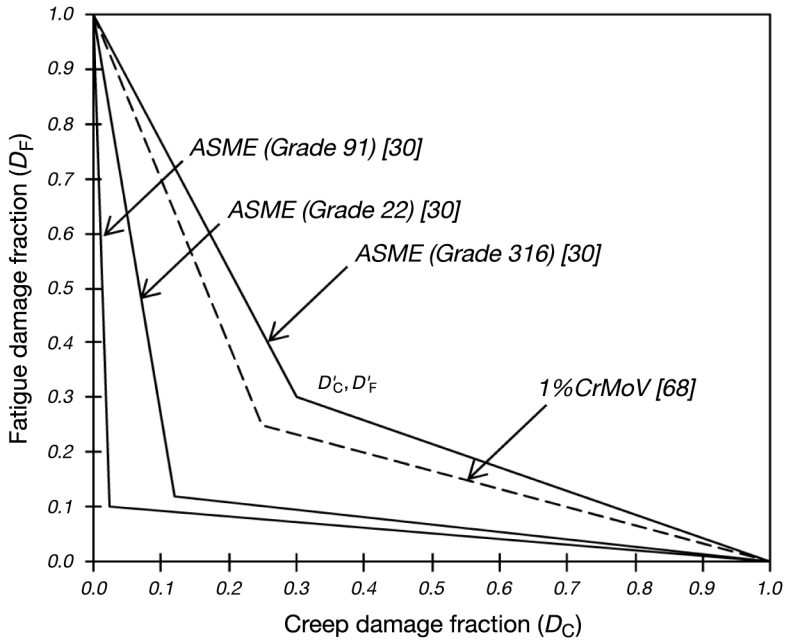

Figure 4-13
Crack initiation loci for different materials

5 Discussion

5.1 Material Property Data Requirements

The main goal of this report has been to review material property data requirements for the assessment of defect-free components subject to creep-fatigue loading during service duty. Although it is recognized that there are a number of procedures employed for this purpose [30–33], the material property requirements are broadly similar and are derived from a relatively small number of common test types (Section 2). A generic flow diagram representing the analysis route adopted by a number of defect-free creep-fatigue assessment procedures was introduced in Section 1. The material property data required for each of the steps identified in Figure 1-2 and the location in the report where they are considered are summarized in Table 5-1.

Table 5-1
Overview of material property data requirements for creep-fatigue assessment

Assessment Step	Material Property Requirements	Sections
Determination of stress-strain state	Physical and elastic properties	3.1, 3.2
	Cyclic stress-strain data	3.3
	Creep strain data	3.4.1, 3.4.2
	Cyclic stress-relaxation data	3.4.3
Determination of fatigue damage fraction	LCF (without and with hold time) crack initiation endurance data for $T_{C/t} \leq T < T_{max}$	4.1, 4.2
Determination of creep damage fraction	Creep-rupture time data for $T_{C/t} \leq T < T_{max}$	4.1, 4.3.1, 4.3.4
	Creep-rupture ductility data for $T_{C/t} \leq T < T_{max}$	4.3.2
Creep-fatigue damage summation	Low strain rate LCF, cyclic/hold (isothermal and TMF) creep-fatigue test data	4.4

In reviewing the material property data requirements for creep-fatigue assessment, the importance of data pre-assessment and differentiating between creep-fatigue deformation and damage interaction effects, in particular for 9–11% Cr steels, is also recognized.

5.2 Data Pre-Assessment

The importance of data pre-assessment prior to model fitting for creep-fatigue assessment purposes cannot be overstated. It is acknowledged in Appendix A that even traditional steels such as 1CrMoV and Grade 22 are widely used in different metallurgical conditions. In the case of 1CrMoV rotor steel, it is simply because turbine manufacturers in different countries have developed and specified the target chemistry limits, heat treatment procedures, and tensile strength requirements to meet regionally adopted design criteria. In the case of Grade 22, the steel is used in both the annealed conditions and the normalized and tempered conditions for various power plant applications. Even in the normalized and tempered condition, the properties of this steel can vary with product section size as a result of

different air-cooling rates from the nomalizing temperature (for example, see Figure 4-7). It is therefore very important to collate and model creep (and creep-process-influenced) properties from data originating from tests on material of the correct product specification (material pedigree).

Pre-assessment is an important step in the analysis of all material property data, involving (a) characterization of the data in terms of its pedigree, distribution (as a function of test control parameters), and scatter, and (b) data reorganization, if deemed necessary by the findings of (a).

5.3 Creep-Fatigue Interaction

5.3.1 Deformation Versus Damage

Creep-fatigue interaction effects on deformation and damage have been recognized for many years [27, 72, 74]. However, more recently, greater efforts have been made to understand and quantify the effects to improve assessment procedure effectiveness [29]. Much of the early work relating to power plant applications was concerned with low-alloy ferritic steels for which the most significant creep-fatigue interaction effects related to physical damage as depicted in Figure 1-1 (for example, Holdsworth et al. (2007) [71] and Figure 4-10). It is now clear that for the new advanced 9–11% Cr steels, deformation interaction effects might be far more influential (for example, Figures 3-3 and 3-6) [29]. In such circumstances, cyclic stress-strain and creep deformation models need to be more carefully formulated to ensure that interaction effects in this class of steel are not erroneously attributed to damage, as shown in Figure 4-13. The evidence first presented in Holdsworth (2010) [29] to illustrate this misunderstanding is reproduced in Figure 5-1. Plotted in a damage summation diagram, published cyclic/hold creep-fatigue test results for Grade 92 at 625°C [75] appear to exhibit creep-fatigue interaction characteristics that are similar to those of Grade 91 and more extensive than those of 1CrMoV at 550°C (see Figure 5-1, panel a). However, when the same data are compared as a function of crack initiation endurance, it is clear that Grade 91/92 steels are superior to 1CrMoV at 550°C (see Figure 5-1, panel b).

5.3.2 PCD- and PFD-Based Properties

Recent studies have demonstrated the potential advantages of basing fatigue and creep damage calculations on PCD fatigue endurance and PFD creep-rupture models. For example, it has been shown that the use of such test data can lead to D_F,D_C coordinates that are more representative of the actual physical damage condition in a damage summation diagram [29]. Some PCD fatigue endurance and PFD creep-rupture properties are reviewed in Figure 4-5 and Figure 4-10 (for 1CrMoV) and Figure 4-11 (for Grade 316). The approach is demanding in terms of experimental data requirements, but it could provide the solution for more effective creep-fatigue lifetime predictions for certain materials in the future.

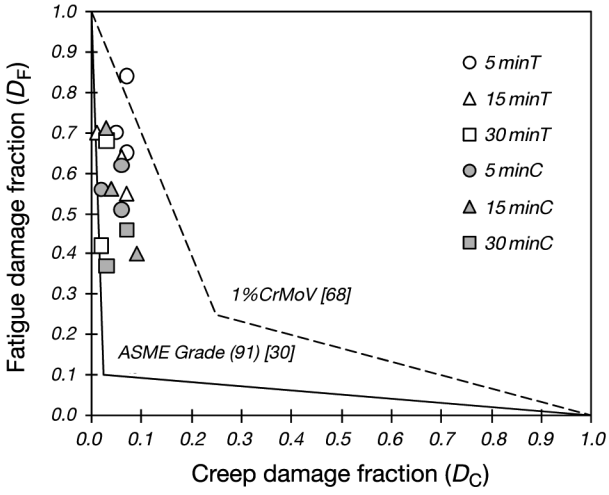

(a)

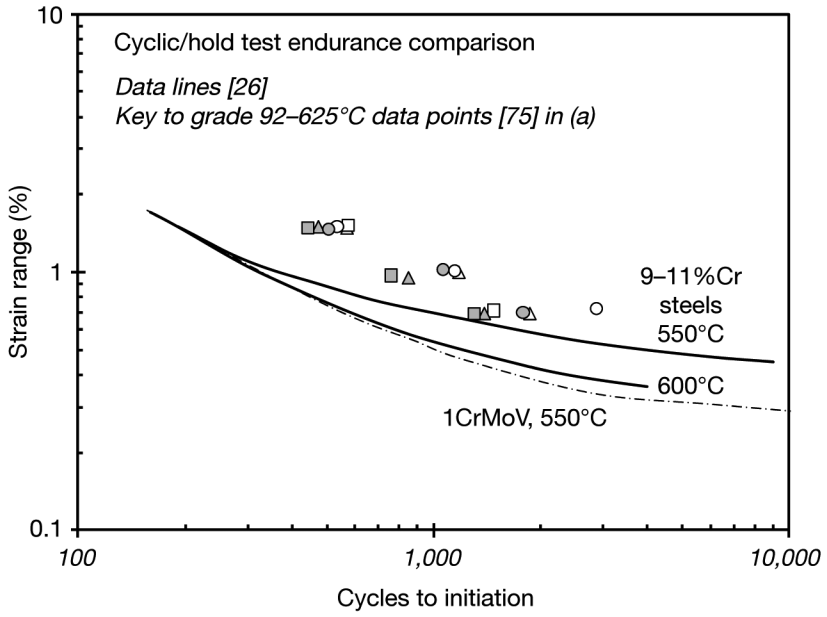

°F = (°C x [9/5]) + 32

(b)

Figure 5-1
Comparison of cyclic/hold creep-fatigue test endurance coordinates for Grade 92 steel at 625°C [75] with (a) the ASME bilinear damage line for Grade 91 [30] and (b) reference endurance lines for 1CrMoV and 9–11% Cr steels [26]

6 References

1. S. R. Holdsworth, "A Knowledge Based System for Creep-Fatigue Assessment," *Nuclear Engineering and Design*, Vol. 188, pp. 289–301 (1999).
2. *EPRI Creep-Fatigue Data Workbook 1: 1CrMoV,* CFdat-1CrMoV-v2.xls (2010).
3. *EPRI Creep-Fatigue Data Workbook 2: 2¼CrMo,* CFdat-Gr22-v2.xls (2010).
4. *EPRI Creep-Fatigue Data Workbook 3: 9CrMoVNb,* CFdat-Gr91-v2.x1s (2010).
5. *EPRI Creep-Fatigue Data Workbook 4: AISI 316,* CFdat-Gr316-v2.xls (2010).
6. *Data Sheets on Elevated-Temperature, Time-Dependent Low-Cycle Fatigue Properties of ASTM A470-8 (1Cr-1Mo-0.25V) Steel Forging for Turbine Rotors and Shafts*, National Research Institute for Metals, Tokyo, Japan, Data Sheet No. 58 (1987).
7. S. Bhongbhibhat, "Parameter-Studie zur Estellung von Dehnungswechselkurven aufgrundverfügbarerErgebnisseausKurzzeitundZeitstandversuchen," *Forschungsberichte, Universität Stuttgart,* Heft 275 (1980).
8. G. Thomas and R. A. T. Dawson, "The Effect of Dwell Period and Cycle Type on High Strain Fatigue Properties of 1CrMoV Rotor Forgings at 500–550°C," *Proceedings of the International Conference on Engineering Aspects of Creep*, Sheffield, Paper C333/80, pp. 167–173 (1980).
9. K. H. Mayer and W. Reiß, "The Influences of the Microstructure on the Operational Characteristics of Steam Turbine Components Subjected to High Stresses," *VGB Kraftwerkstechnik*, No. 4, pp. 138–142 (March 1976).
10. *Data Sheets on Elevated-Temperature, Time-Dependent Low-Cycle Fatigue Properties of SCMV (2.25Cr-1Mo) Steel Plate for Pressure Vessels*, National Research Institute for Metals, Tokyo, Japan, Data Sheet No. 62 (1989).
11. *Data Sheet on Long-Term, High Temperature Low-Cycle Fatigue Properties of SCMV 4 (2.25Cr-1Mo) Steel Plate for Boilers and Pressure Vessels*, National Institute for Materials Science, Japan, Data Sheet No. 94 (2004).
12. *Data Sheets on Elevated-Temperature Time-Dependent Low-Cycle Fatigue Properties of ASTM A387 Grade 91 (9Cr-1Mo) Steel Plate for Pressure Vessels*, National Research Institute for Metals, Tokyo, Japan, Data Sheet No. 78 (1993).
13. Y. Takahashi, "Study on Creep-Fatigue Evaluation Procedures for High-Chromium Steels—Part I: Test Results and Life Prediction Based on Measured Stress Relaxation," *International Journal of Pressure Vessels & Piping*, Vol. 85, pp. 406–422 (2008).
14. *Data Sheets on Elevated-Temperature, High-Cycle and Low-Cycle Fatigue Properties of SUS316-HP (18Cr-12Ni-2Mo) Hot Rolled Stainless Steel Plate*, National Research Institute for Metals, Tokyo, Japan, Data Sheet No. 15 (1979).
15. C. R. Brinkman et al., "Long Term Creep-Fatigue Tests on Type 316FR Stainless Steel," ORNL/316FR/94-2, Oak Ridge National Laboratory (September 1994).
16. C. R. Brinkman, "Elevated-Temperature Mechanical Properties of an Advanced Type 316 Stainless Steel," in *Advances in Life Prediction Methodology*, PVP-Vol. 391, American Society of Mechanical Engineers, New York, pp. 87–94 (1999).

17. J. B. Conway, R. H. Stentz, and J. T. Berling, "Fatigue, tensile and relaxation behaviour of stainless steels," TID-26135, Technical Information Centre USAEC (1975).

18. *Data Sheets on the Elevated-Temperature Properties of 1Cr-1Mo-0.25V Steel Forgings for Turbine Rotors and Shafts (ASTM A470-8)*, National Research Institute for Metals, Tokyo, Japan, Data Sheet No. 9B (1990).

19. *Data Sheets on the Elevated-Temperature Properties of 2.25Cr-1Mo Steel (various product forms)*, National Research Institute for Metals, Tokyo, Japan, Data Sheet Nos. 3B (1986), 11B (1997), 36B (2003).

20. *Data Sheets on the Elevated-Temperature Properties of 9Cr-1Mo-V-Nb Steel Tubes for Boilers and Heat Exchangers (ASME SA-213/SA-213M Grade 91) and 9Cr-1Mo.V.Nb Steel Plates for Boilers and Pressure Vessels (ASME SA-387/SA-387M Grade 91)*, National Research Institute for Metals, Tokyo, Japan, Data Sheet No. 43 (1996).

21. *Data Sheets on the Elevated-Temperature Properties of 18Cr-12Ni-Mo Stainless Steel (various product forms)*, National Research Institute for Metals, Tokyo, Japan, Data Sheet Nos. 6B (2000), 14B (1988), 15B (1988), 42 (1996).

22. K. Yagi, G. Merckling, T.-U. Kern, H. Irie, and H. Warlimont (eds.), *Landolt-Börnstein: Numerical Data and Functional Relationships in Science and Technology, Group VIII: Advanced Materials and Technologies, Volume 2, Materials, Subvolume B, Creep properties of Heat Resistant Steels*, Berlin: Springer-Verlag, (2004).

23. D. G. Robertson and S. R. Holdsworth (eds.), *Rupture Strength, Creep Strength and Relaxation Strength Values for Carbon-Manganese, Low Alloy Ferritic, High Alloy Ferritic and Austenitic Steels, Nickel Base Alloys and High Temperature Bolting Alloys*. European Creep Collaborative Committee (ECCC) Data Sheets: (2005) http://www.ommi.co.uk/etd/eccc/advancedcreep/open.htm.

24. S. R. Holdsworth and D. Gandy, "Towards a Standard for Creep-Fatigue Testing," *Proceedings of the 5th International Conference on Advances in Materials Technology for Fossil Power Plants*, EPRI, Marco Island, FL, USA (October 2007).

25. ASTM E2714, "Standard Test Method for Creep-Fatigue Testing," *ASTM Standards*, Vol. 03.01 (2009).

26. S. R. Holdsworth, "Creep-Fatigue of High Temperature Turbine Steels," *Materials at High Temperatures*, Vol. 18, No. 4, pp. 261–265 (2001).

27. D. Miller, R. H. Priest, and E. G. Ellison, "A Review of Material Response and Life Prediction Techniques," *High Temperature Material Processes*, Vol. 6, Nos. 3/4, pp. 155–194 (1984).

28. V. Bicego, C. Fosati, and S. Ragazonni, "Low Cycle Fatigue Characterization of a HP-IP Steam Turbine Rotor," in *Low Cycle Fatigue*, Philadelphia, ASTM STP942, pp. 1237–1260 (1988).

29. S. R. Holdsworth, "Creep-Fatigue in Steam Turbine Materials," *Proceedings of the 6th International Conference on Advances in Materials Technology for Fossil Power Plants*, EPRI, Santa Fe, NM, USA (September 2010).

30. ASME, "Rules for the Construction of Nuclear Facility Components, Class 1 Components in Elevated Temperature Service, Boiler and Pressure Code, Section III, Division 1—Subsection NH" (2001).

31. TRD 301, "Annex I—Design: Calculation for Cyclic Loading due to Pulsating Internal Pressure or Combined Changes of Internal Pressure and Temperature," *in Technical Rules for Steam Boilers* (1978).

32. RCC-MR, *Design and Construction Rules for Mechanical Components of FBR Nuclear Islands, Section I—Nuclear Islands Components* Edition. AFCEN (1985).

33. R. A. Ainsworth, et al. (eds.), R5, *An Assessment Procedure for the High Temperature Response of Structures*, Barnwood: British Energy Generation (2003).

34. G. R. Halford and S. S. Manson, "Life Prediction of Thermal Mechanical Fatigue Using Strain Range Partitioning," in *Thermal Fatigue of Materials and Components*, ASTM STP 612, eds. D. A. Spera and D. F. Mowbray, pp. 239–54 (1976).

35. W. Hoffelner, "Creep-Fatigue Life Determination of Grade 91 Steel Using Strain-Range Separation Method," *Proceedings of the ASME Pressure Vessel and Piping Conference*, PVP2009-77705 (2009).

36. M. Prager, "Extended Low Chrome Steel Fatigue Rules," STP-PT-027, ASME Standards Technology, LLC (2009).

37. ISO 12106, "Metallic Materials—Fatigue Testing—Axial-Strain-Controlled Method," International Organization for Standardization (2003).

38. E. Mazza, M. Hollenstein, S. R. Holdsworth, and R. P. Skelton, "Notched Specimens Thermo-Mechanical Fatigue of a 1CrMoV Turbine Steel," *Nuclear Engineering and Design*, Vol. 234, pp. 11–24 (2004).

39. EN 10291, "Metallic Materials—Uniaxial Creep Testing in Tension—Method of Test, European Norm" (2001).

40. M. Gerland et al., "Low Cycle Fatigue Behaviour in Vacuum of a 316L Austenitic Stainless Steel Between 20 and 600°C—Part II: Dislocation Structure Evolution and Correlation With Cyclic Behaviour," *Materials Science and Engineering*, Vol. A229, pp. 68–86 (1997).

41. SEW 310, "Physikalische Eigenschaften von Stählen," *Stahl-Eisen-Werkstoffblätter des Vereins Deutscher Eisenhüttenleute* (1992).

42. G. Maier, "Untersuchungen zum Elastizitätsmodul von Stählen bei höheren Temperaturen," *Materialprüfung*, Band 29, Nr. 11/12, Dezember, pp. 358–366 (1987).

43. M. Radosavljevic and S. R. Holdsworth, "Elastic Modulus Determination Method for Evaluation of Material Response Under Cyclic Loading Conditions," (submitted).

44. R. Hales, S. R. Holdsworth, M. P. O'Donnel, I. J. Perrin, and R. P. Skelton, "A Code of Practice for the Determination of Cyclic Stress-Strain Data," *Materials at High Temperatures*, Vol. 19, No. 4, pp. 165–185 (2002).

45. J. L. Chaboche, "A Review of Some Plasticity and Viscoplasticity Constitutive Theories," *International Journal of Plasticity*, Vol. 24, No. 10, pp. 1642–1693 (2008).

46. C. E. Pugh et al., "Currently Recommended Constitutive Equations for Inelastic Design Analysis of FFTE Components," ORNL-TM-3602 (1972).

47. J. Lemaitre and J. L. Chaboche, *Mechanics of Solid Materials*, Cambridge University Press (1990).

48. *Abaqus Analysis User's Manual*. Simulia (2010).

49. W. Ramberg and W. R. Osgood, "Description of Stress Strain Curves by Three Parameters," NASA TN-902 (1946).

50. S. R. Holdsworth, "Constitutive Equations for Creep Curves and Predicting Service," in *Creep-Resistant Steels*, eds. F Abe, T.-U. Kern & R. Viswanathan, pp. 403–420 Woodhead (2008).

51. F. N. Norton, *The Creep of Steel at High Temperature*, McGraw-Hill (1929).

52. J. L. Bolton, "A 'Characteristic Strain' Model for Creep," in *Proceedings of the ECCC Creep Conference on Creep & Fracture in High Temperature Components—Design & Life Assessment Issues, Journal of the Institute of Metals*, London, eds. I. A. Shibli, S. R. Holdsworth, and G. Merckling, pp. 465–477 (September 2005).

53. P. Feltham, "Stress Relaxation in Copper and Alpha Brasses at Low Temperatures," *Journal of the Institute of Metals*, Vol. 98, p. 210 (1960).

54. L. F. Coffin, "A Note on Low Cycle Fatigue Laws," *Journal of Materials*, Vol. 6, No. 2, p. 388 (1971).

55. B. F. Langer, "Design of pressure vessels for low cycle fatigue," *Journal of Basic Engineering*, Series D, Trans ASME, Vol. 84, p. 389 (1962).

56. M. Reigl and D. N. Harish, "Considerations to the an-isothermal creep-fatigue assessment of steam turbine rotor steels," *Proceedings of the 8th International Conference on Creep and Fatigue at Elevated Temperatures, CREEP8*, San Antonio, Texas, PVP2007-26553 (July 2007).

57. N. Shinya, J. Kyono, H. Kushima, and S. Yokoi, "Effect of creep damage on fatigue life of Cr Mo V steel," *Transactions of the National Research Institute for Metals*, Vol. 29, No. 2, pp. 115–123 (1987).

58. L. Binda, S. R. Holdsworth and E. Mazza, "Creep-Fatigue Damage Characterisation," *Proceedings of the 6th International Conference on Low Cycle Fatigue* (LCF6), Berlin, Germany, pp. 333–338 (September 2008).

59. S. R. Holdsworth, "Advances in the Assessment of Creep Data," *Proceedings of the 9th Liège Conference on Materials for Advanced Power Engineering*, Liège, Belgium (September 2010).

60. A. Mendelson, E. Roberts, and S. S. Manson, "Optimization of Time-Temperature Parameters for Creep and Stress Rupture with Application to Data from German Cooperative Long-Time Creep Program," NASA-TN-D-2975 (August 1965).

61. I. I. Trunin, N. G. Golobova, and E. A. Loginov, "New Method of Extrapolation of Creep Test and Long Time Strength Results," in *Proceedings of the 4th International Symposium on Heat Resistant Metallic Materials*, Mala Fatra, CSSR, p. 168 (1971).

62. B. Wilshire and P. J. Scharning, " A New Methodology for Analysis of Creep and Creep Fracture Data for 9–12% Chromium Steels," *International Material Reviews*, Vol. 53, No. 2, pp. 91–104 (2008).

63. S. R. Holdsworth, "Developments in the Assessment of Creep Strain and Ductility Data," *Materials at High Temperatures*, Vol. 21, No. 1, pp. 25–31 (2004).

64. M. W. Spindler, "The Multiaxial and Uniaxial Creep Ductility of Type 304 Steel as a Function of Stress and Strain Rate," *Materials at High Temperatures*, Vol. 21, No. 1, pp. 47–54 (2004).

65. W. M. Payten, D. W. Dean, and K. U. Snowden, " A Strain Energy Density Method for the Prediction of Creep Fatigue Damage in High Temperature Components," *Materials Science & Engineering*, (2010).

66. L. Binda, S. R. Holdsworth, and E. Mazza, "Influence of Prior Cyclic Deformation on Creep Properties of 1CrMoV," *Materials at High Temperatures*, Vol. 27, No. 1, pp. 21–27 (2010).

67. L. Binda, *Advanced Creep Damage and Deformation Assessment of Materials Subject to Steady and Cyclic Loading at High Temperatures*, DSc Thesis, DISS. ETH No. 18462, Zürich (2010).

68. S. R. Holdsworth, "Prediction of Creep-Fatigue Behaviour at Stress Concentrations in 1CrMoV Rotor Steel," *Proceedings of the Conference on Life Assessment and Life Extension of Engineering Plant Structures and Components*, Churchill College, Cambridge, pp. 137–146 (September 1996).

69. R. D. W. Bestwick and A. Clayton, "A Design Methodology for Creep-Fatigue Assessment Using Creep Ductility Criteria," in *Proceedings of the 5th International Seminar on Inelastic Analysis and Life Prediction in High Temperature Environment*, Paris, 1985, pp. 55–60.

70. R. P. Skelton and D. Gandy, "Creep-Fatigue Damage Accumulation and Interaction Diagram Based on Metallographic Interpretation of Mechanisms," *Materials at High Temperatures*, Vol. 25, No. 1, pp. 27–54 (2008).

71. S. R. Holdsworth, E. Mazza, L. Binda, and L. Ripamonti, "Development of Thermal Fatigue Damage in 1CrMoV Rotor Steel," *Nuclear Engineering and Design*, Vol. 237, No. 4, 2292–2301 (2007).

72. D. P. Timo, "Designing Turbine Components in Fatigue," *Proceedings of the International Conference on Thermal Stresses and Fatigue*, Berkeley, UK, pp. 453–469 (September 1969).

73. R. A. T. Dawson, "Monitoring and Control of Thermal Stress and Component Life Expenditure in Steam Turbines," *Proceedings of the International Conference on Modern Power Stations*, AIM, Liège (1989).

74. M. M. Leven, "The Interaction of Creep and Fatigue for Rotor Steels," Experimental Mechanics, September, pp. 353–372 (1973).

75. M. Sato et al, "Creep-Fatigue Characteristics of Advanced High Strength Cr-W Steels for Power Boiler Applications," *Proceedings of the Conference on Advanced Heat Resistant Steels for Power Generation*, IOM, UK, pp. 298–308 (1999).

A EPRI Creep-Fatigue Data Workbooks

A.1 Overview

The EPRI creep-fatigue data workbooks are based on the concept introduced in [1]. This involves the storage of creep-fatigue data on three levels, that is, experimentally determined data reduced to a manageable quantity (Level 1), summary data (Level 2), and assessed data (Level 3).

Data workbooks have been established for four steels, namely 1CrMoV [2], 2¼CrMo (Grade 22) [3], 9CrMoVNb (Grade 91) [4], and Grade 316 [5]. They comprise data from a number of sources [6–17].

A.2 Creep-Fatigue Data

The data workbooks contain LCF, cyclic/hold creep-fatigue test, and creep-rupture data (see Figure A-1). Priority is given to the storage of LCF and cyclic/hold creep-fatigue test data. However, the workbooks are also used for the collation of creep-rupture data, in particular when it exists for the same heats of material as for the cyclic data. There are other sources of creep-rupture data that were not exploited because the information did not relate directly to the heats of steel for which LCF and cyclic/hold creep-fatigue test data had been collated [18–22]. The assessment of these data has been reported elsewhere [23].

Cycle shapes showing the main control and response variables for commonly adopted cyclic/hold creep-fatigue tests providing the data contained in the workbooks are given in Figure A-2. In the case of LCF tests, the hold time is zero (that is, t_h = 0 h). LCF waveforms are invariably triangular, usually with a strain rate of 0.001/s, although data are stored for tests employing strain rates as low as 1×10^{-7}/s.

A.3 Data Workbook Structure

During a creep-fatigue test, control and response variables are saved as a function of time and cycle number, usually for selected cycles (but sometimes for all cycles) [24, 25]. In the past, it was usual to record this information by hand and using $X(t)$ and X-$Y(t)$ chart recorders. Now it is more common to record such observations using a digital acquisition system. The quantity of information collected by the laboratory for a given test is usually far more than is required for subsequent assessment purposes, and therefore the information is usually retained and stored by the original test laboratory such that data analysts can access it if more details are required at a later date.

For subsequent analysis, for example, to determine the parameters for constitutive model equations to be used as material property input in component assessment, it is more convenient to reduce the deformation data set in particular to a size that is more convenient for analysis. Individual creep-fatigue test deformation (Level 1) data and test summary (Level 2) data are held in different sheets of the data workbook as introduced next.

Reduced (Level 1) data for individual tests are stored in blocks of cells in the *cyclic stress-strain records* and *cyclic stress-relaxation records* sheets.

In the cyclic stress-strain records sheet, it is recommended that stress-strain records for a given cycle comprise no more than ~200 (ε,σ) data points, collected in a way to adequately characterize the shape of the hysteresis loop at all locations (see Figure A-3). Ideally, the (ε,σ) data points should be equispaced around the cyclic part of the loop. A predefined scheme is recommended for storage of the hold time $\sigma(t)$ data in the *cyclic stress-relaxation records* sheet (see Figure A-4).

Summary (Level 2) data sheets contain summary data for a number of tests in individual rows. There are two summary data sheets, one for *LCF and cyclic/hold fatigue properties* (see Figure A-5) and one for *creep-rupture properties* (see Figure A-6). The data stored in summary data sheets summarize results from the reduced data sheets as well as information from other sources. Each row in a summary data sheet summarizes the results from one test.

Assessed (Level 3) data is information from reduced data and summary data sheets expressed in constitutive and model equation format. This form of representation provides a convenient means of continuous material property data input into component assessment calculations.

A.4 Data Workbooks

The contents of the four version 2 data workbooks [2–5] are summarized in tables in the following sections.

A.4.1 1CrMoV

1CrMoV has been widely used since the 1960s as a high-pressure and intermediate-pressure steam turbine rotor steel for inlet temperatures up to 565°C. Consequently, there is a significant quantity of creep-fatigue property data available for the steel [6–8]. Care is required when using the available data, because the steel is used in subtly different conditions by different turbine manufacturers in different parts of the world, despite the nominal specifications for the steel being almost identical. For example, the chemical compositional balance of the steel and the heat treatment procedure adopted in mainland Europe has tended to evolve in a different way from that in the United Kingdom. This steel typically exhibits an inverse relationship between creep-rupture strength and fracture toughness [9]. Mainland European turbine makers tended to optimize rotor manufacturing practice in favor of fracture toughness, whereas UK turbine makers tended to favor superior creep properties. Similarly, there can be differences between the compositional balance and heat treatment procedures adopted for U.S. variants to ASTM (formerly, the American Society for Testing and Materials) A470.

The contents of the *1CrMoV Creep-Fatigue Data Workbook* [2] are summarized in Table A-1.

Table A-1
Summary of the contents of the Creep-Fatigue Data Workbook 1: 1CrMoV [2]

	Casts	LCF Tests	Cyclic/Hold Tests	Creep-Rupture Tests
Total	4	106 (5)	119 (8)	14
RT	1	7 (1)		
400°C	1	6 (1)		
500°C	2	38* (1)	26 (4)	5
525°C	1		10	
530°C	1	9	18	
550°C	2	39* (1)	65 (4)	6
600°C	1	7 (1)		3

Note: Numbers in parentheses are numbers of tests for which there are deformation data in the workbook.
* Including low-strain-rate test data.

A.4.2 2¼CrMo (Grade 22)

2¼CrMo (Grade 22) has also been widely adopted for many years in the power generation industry as a main and boiler steam pipe material, also for temperatures up to ~550°C. There are data in the *Creep-Fatigue Data Workbook* for this steel [3] from published [10, 11] and unpublished sources. Care is also required in the use of available data for Grade 22, because it is commonly employed in both the annealed and normalized and tempered conditions. In the annealed condition, the microstructure is typically fully ferritic, whereas in the normalized condition, microstructures range from fully bainitic in relatively thin section product forms to mixed ferrite/bainite in thicker section product forms. The microstructure and initial strength conditions have a significant influence on fatigue and creep properties.

The contents of the Grade 22 *Creep-Fatigue Data Workbook* are summarized in Table A-2.

Table A-2
Summary of the contents of the Creep-Fatigue Data Workbook 2: 2¼CrMo [3]

	Casts	LCF Tests	Cyclic/Hold Tests	Creep-Rupture Tests
Total	13	478	92	46
RT	4	36		
93°C	1	1		
300°C	2	13		
316°C	2	26		
371°C	2	12		
400°C	2	17		
427°C	5	47		
454°C	3	3		3
482°C	3	24	20	1
500°C	2	42*	11	3
510°C	1			9
538°C	8	128*	33	13
550°C	1			4
566°C	1	4		6
593°C	5	74*	18	
600°C	2	51*	10	7

Note: Numbers in parentheses are numbers of tests for which there are deformation data in the workbook.
* Including low-strain-rate test data.

A.4.3 9CrMoVNb (Grade 91)

Since the development of the modified 9CrMo steel in the 1980s, Grade 91 (9CrMoVNb) has been widely used as an alternative to Grade 22 for power plant tube and pipe applications when higher temperature creep and oxidation resistance are required or when thinner wall sections are required at temperatures up to ~550°C. Grade 91 is typically used for high temperature applications to ~575-600°C. Grade 91 is used for many other purposes in the power generation industry, notably as a boiler header and turbine casting steel, and there are a number of sources of creep-fatigue properties [12,13]. The contents of the Grade 91 *Creep-Fatigue Data Workbook* [4] are summarized in Table A-3.

Hold times up to 60 minutes in both tension and/or compression. The maximum hold time in tension is 180 minutes.

Table A-3
Summary of the contents of the Creep-Fatigue Data Workbook 3: 9CrMoVNb [4]

	Casts	LCF Tests	Cyclic/Hold Tests	Creep-Rupture Tests
Total	8	296	85 (1)	103
RT	4	44		
371°C	3	18		
427°C	1			2
454°C	1			1
482°C	3	21	2	3
500°C	2	6		7
538°C	5	54	19	25
550°C	2	41*	23 (1)	11
593°C	5	59	21	34
600°C	2	41*	12	8
650°C	3	12	8	12

Note: Numbers in parentheses are numbers of tests for which there are deformation data in the workbook.
* Including low-strain-rate test data.

A.4.4 Grade 316

Grade 316 (18Cr12Ni2Mo) has been employed widely in the power generation industry since the 1960s for high temperatures up to ~650°C. It exhibits a high resistance to creep and oxidation at temperatures well above those of the ferritic and martensitic steels. Creep-fatigue data has been gathered from [14–17]. The contents of the Grade 316 *Creep-Fatigue Data Workbook* [5] are summarized in Table A-4.

Table A-4
Summary of the contents of the Creep-Fatigue Data Workbook 4: AISI 316 [5]

	Casts	LCF Tests	Cyclic/Hold Tests	Creep-Rupture Tests
Total	7	347	81	16
RT	2	19		
400°C	1	16*		
450°C	1	6		
500°C	6	72*	4	
550°C	5	99*	45	2
600°C	4	67*	32	8
650°C	1	29*		3
700°C	1	16*		3
817°C	1	23*		

Note: Numbers in parentheses are numbers of tests for which there are deformation data in the workbook.
* Including low-strain-rate test data.

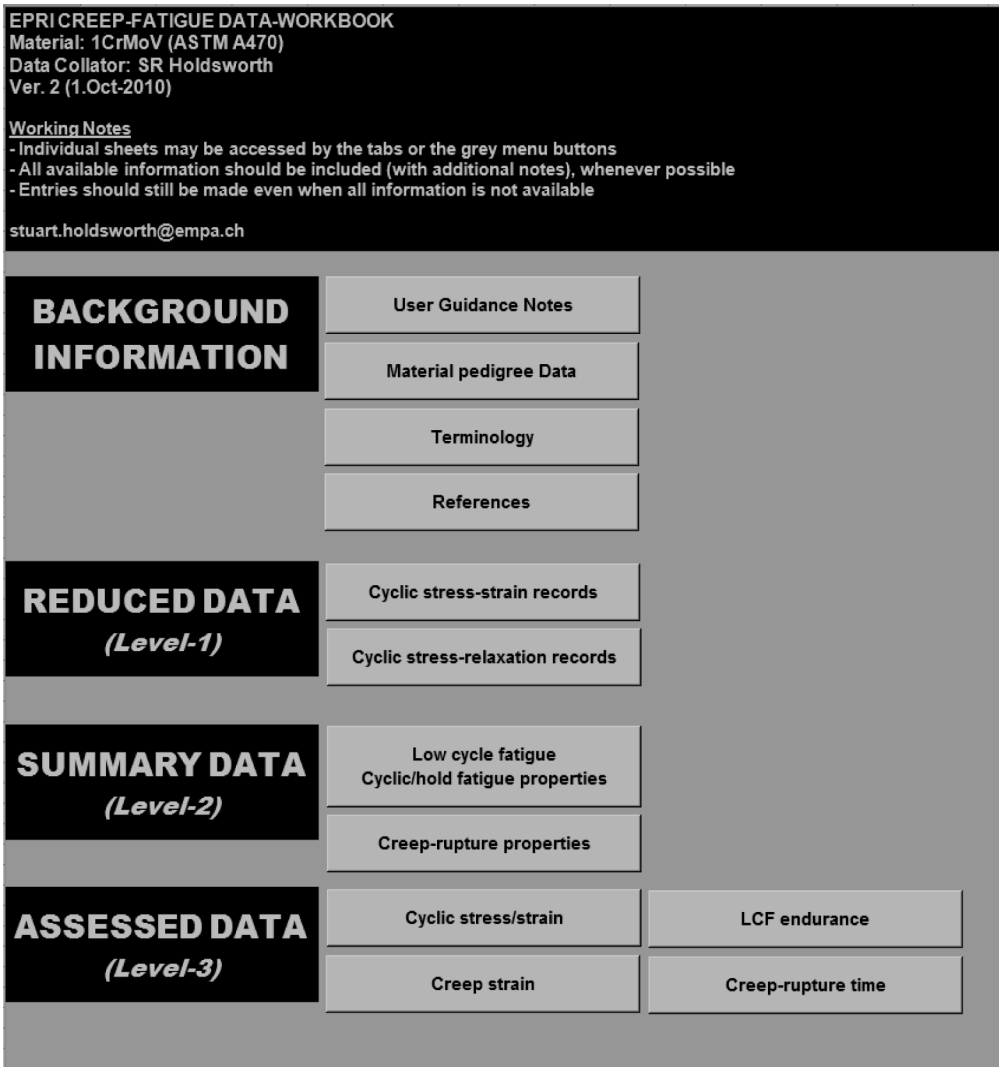

Figure A-1
Appearance of the contents sheet of the Creep-Fatigue Data Workbook (version 2)

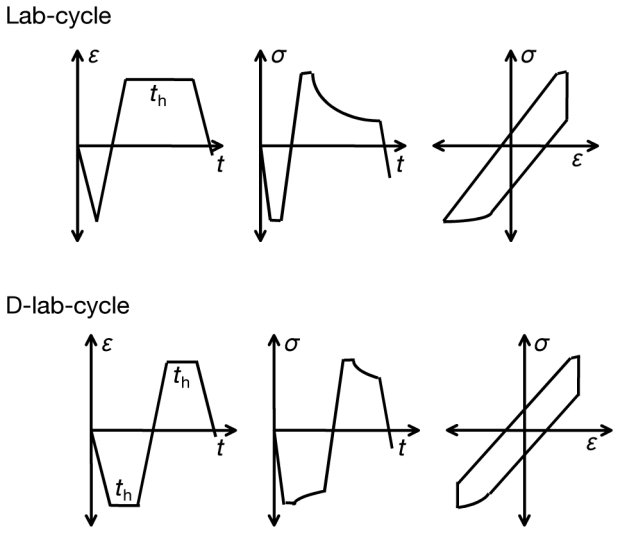

Figure A-2
Commonly used isothermal strain-controlled cyclic/hold creep-fatigue test cycle shapes [26]

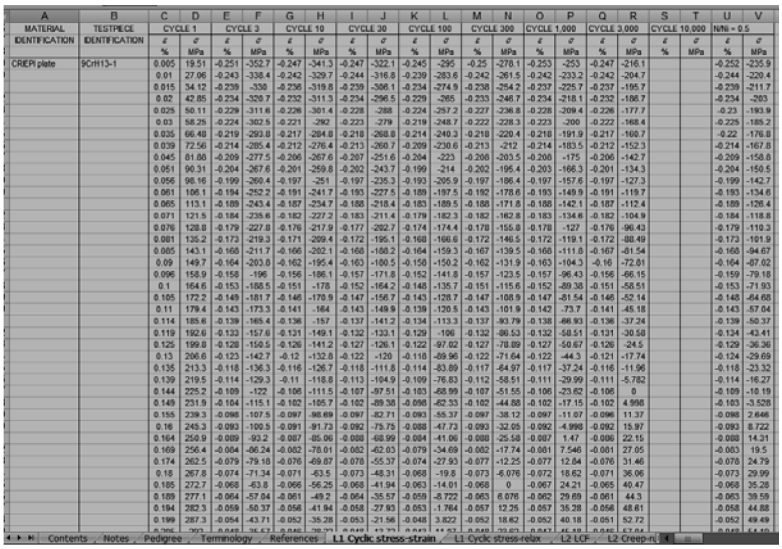

MATERIAL IDENTIFICATION	TESTPIECE IDENTIFICATION	CYCLE 1		CYCLE 3		CYCLE 10		CYCLE 30		CYCLE 100		CYCLE 300		CYCLE 1,000		CYCLE 3,000		CYCLE 10,000		N/Ni = 0.5	
		ε %	σ MPa	ε %	σ MPa	ε %	σ MPa	ε %	σ MPa	ε %	σ MPa	ε %	σ MPa	ε %	σ MPa	ε %	σ MPa	ε %	σ MPa	ε %	σ MPa
CREPI plate	9Cr1i13-1	0.005	19.51	-0.251	-352.7	-0.247	-341.3	-0.247	-322.1	-0.245	-295	-0.25	-278.1	-0.253	-253	-0.247	-216.1			-0.252	-235.9
		0.01	27.06	-0.243	-338.4	-0.242	-329.7	-0.244	-316.8	-0.239	-283.6	-0.242	-261.5	-0.242	-233.2	-0.242	-204.7			-0.244	-220.4
		0.015	34.12	-0.239	-330	-0.236	-319.8	-0.239	-306.1	-0.234	-274.9	-0.238	-254.2	-0.237	-225.7	-0.237	-195.7			-0.239	-211.7
		0.02	42.85	-0.234	-326.7	-0.232	-311.3	-0.234	-296.5	-0.229	-265	-0.233	-246.7	-0.234	-218.1	-0.232	-186.7			-0.234	-203
		0.025	50.11	-0.229	-311.6	-0.226	-301.4	-0.228	-288	-0.224	-257.2	-0.227	-236.8	-0.228	-209.4	-0.226	-177.7			-0.23	-193.9
		0.03	58.25	-0.224	-302.5	-0.221	-292	-0.223	-279	-0.219	-248.7	-0.222	-228.3	-0.223	-200	-0.222	-168.4			-0.225	-185.2
		0.035	66.48	-0.219	-293.8	-0.217	-284.8	-0.218	-268.8	-0.214	-240.3	-0.218	-220.4	-0.218	-191.9	-0.217	-160.7			-0.22	-176.8
		0.039	72.56	-0.214	-285.4	-0.212	-276.4	-0.213	-260.7	-0.209	-230.6	-0.213	-212	-0.214	-183.5	-0.212	-152.3			-0.214	-167.8
		0.045	81.88	-0.209	-277.5	-0.206	-267.6	-0.207	-251.6	-0.204	-223	-0.208	-203.5	-0.208	-175	-0.206	-142.7			-0.209	-158.6
		0.051	90.31	-0.204	-267.6	-0.201	-259.8	-0.202	-243.7	-0.199	-214	-0.202	-195.4	-0.203	-166.3	-0.201	-134.3			-0.204	-150.5
		0.056	98.16	-0.199	-260.4	-0.197	-251	-0.197	-235.3	-0.193	-205.9	-0.197	-186.4	-0.197	-157.6	-0.197	-127.3			-0.199	-142.7
		0.061	106.1	-0.194	-252.2	-0.191	-241.7	-0.193	-227.5	-0.189	-197.5	-0.192	-178.6	-0.193	-149.9	-0.191	-119.7			-0.193	-134.6
		0.065	113.1	-0.189	-243.4	-0.187	-234.7	-0.188	-218.4	-0.183	-189.5	-0.188	-171.8	-0.188	-142.1	-0.187	-112.4			-0.189	-126.4
		0.071	121.5	-0.184	-235.6	-0.182	-227.2	-0.183	-211.4	-0.179	-182.3	-0.182	-162.8	-0.183	-134.6	-0.182	-104.9			-0.184	-118.8
		0.076	128.8	-0.179	-227.8	-0.176	-217.9	-0.177	-202.7	-0.174	-174.4	-0.178	-155.8	-0.178	-127	-0.176	-96.43			-0.179	-110.3
		0.081	135.2	-0.173	-219.3	-0.171	-209.4	-0.172	-195.1	-0.168	-166.6	-0.172	-146.5	-0.172	-119.1	-0.172	-88.49			-0.173	-101.9
		0.085	143.1	-0.168	-211.7	-0.166	-202.1	-0.168	-188.2	-0.164	-159.3	-0.167	-139.5	-0.166	-111.8	-0.167	-81.54			-0.168	-94.67
		0.09	149.7	-0.164	-203.8	-0.162	-195.4	-0.163	-180.5	-0.158	-150.2	-0.162	-131.9	-0.163	-104.3	-0.16	-72.81			-0.164	-87.02
		0.096	158.9	-0.158	-196	-0.156	-186.1	-0.157	-171.8	-0.152	-141.8	-0.157	-123.5	-0.157	-96.43	-0.156	-66.15			-0.159	-79.18
		0.1	164.6	-0.153	-188.5	-0.151	-178	-0.152	-164.2	-0.148	-135.7	-0.151	-115.6	-0.152	-89.38	-0.151	-58.51			-0.153	-71.93
		0.105	172.2	-0.149	-181.7	-0.146	-170.9	-0.147	-156.7	-0.143	-128.7	-0.147	-108.9	-0.147	-81.54	-0.146	-52.14			-0.148	-64.68
		0.11	179.4	-0.143	-173.3	-0.141	-164	-0.143	-149.9	-0.139	-120.5	-0.143	-101.9	-0.142	-73.7	-0.141	-45.18			-0.143	-57.04
		0.114	185.6	-0.139	-165.4	-0.136	-157	-0.137	-141.2	-0.134	-113.3	-0.137	-93.79	-0.138	-66.93	-0.136	-37.24			-0.139	-50.37
		0.119	192.6	-0.133	-157.6	-0.131	-149.1	-0.132	-133.1	-0.129	-106	-0.132	-86.53	-0.132	-59.51	-0.131	-30.58			-0.134	-43.41
		0.125	199.8	-0.128	-150.5	-0.126	-141.2	-0.127	-126.1	-0.122	-97.62	-0.127	-78.89	-0.127	-50.67	-0.126	-24.5			-0.129	-36.36
		0.13	206.6	-0.123	-142.7	-0.12	-132.8	-0.122	-120	-0.118	-89.96	-0.122	-71.64	-0.122	-44.3	-0.121	-17.74			-0.124	-29.69
		0.135	213.3	-0.118	-136.3	-0.116	-126.7	-0.118	-111.8	-0.114	-83.89	-0.117	-64.97	-0.117	-37.24	-0.116	-11.96			-0.118	-23.32
		0.139	219.5	-0.114	-129.3	-0.11	-118.8	-0.113	-104.9	-0.109	-76.83	-0.112	-58.51	-0.111	-29.99	-0.111	-5.782			-0.114	-16.27
		0.144	225.2	-0.109	-122	-0.106	-111.5	-0.107	-97.51	-0.103	-68.99	-0.107	-51.55	-0.106	-23.62	-0.106	0			-0.109	-10.19
		0.149	231.9	-0.104	-115.1	-0.102	-105.7	-0.102	-89.38	-0.098	-62.33	-0.102	-44.88	-0.102	-17.15	-0.102	4.998			-0.103	-3.528
		0.155	239.3	-0.098	-107.5	-0.097	-98.69	-0.097	-82.71	-0.093	-55.37	-0.097	-38.12	-0.097	-11.07	-0.096	11.37			-0.098	2.646
		0.16	245.3	-0.093	-100.5	-0.091	-91.73	-0.092	-75.75	-0.088	-47.73	-0.093	-32.05	-0.092	-4.998	-0.092	15.97			-0.093	8.722
		0.164	250.9	-0.089	-93.2	-0.087	-85.06	-0.088	-68.99	-0.084	-41.06	-0.088	-25.58	-0.087	1.47	-0.086	22.15			-0.088	14.31
		0.169	256.4	-0.084	-86.24	-0.082	-78.01	-0.082	-62.03	-0.079	-34.69	-0.082	-17.74	-0.081	7.546	-0.081	27.05			-0.083	19.5
		0.174	262.5	-0.079	-79.18	-0.076	-69.87	-0.078	-55.37	-0.074	-27.93	-0.077	-12.25	-0.077	12.84	-0.076	31.46			-0.078	24.79
		0.18	267.8	-0.074	-71.34	-0.071	-63.5	-0.073	-48.31	-0.068	-19.8	-0.073	-6.076	-0.072	18.62	-0.071	36.06			-0.073	29.99
		0.185	272.7	-0.068	-63.8	-0.066	-56.25	-0.068	-41.94	-0.063	-14.01	-0.068	0	-0.067	24.21	-0.065	40.47			-0.068	35.28
		0.189	277.1	-0.064	-57.04	-0.061	-49.2	-0.064	-35.57	-0.059	-8.722	-0.063	6.076	-0.062	29.69	-0.061	44.3			-0.063	39.59
		0.194	282.3	-0.059	-50.37	-0.056	-41.94	-0.058	-27.93	-0.053	-1.764	-0.057	12.25	-0.057	35.28	-0.056	48.61			-0.058	44.88
		0.199	287.3	-0.054	-43.71	-0.052	-35.28	-0.053	-21.56	-0.048	3.822	-0.052	18.62	-0.052	40.18	-0.051	52.72			-0.052	49.49

Contents | Notes | Pedigree | Terminology | References | L1 Cyclic stress-strain | L1 Cyclic stress-relax | L2 LCF | L2 Creep-Fa

Figure A-3
Appearance of the L1 cyclic stress-strain sheet of the Creep-Fatigue Data Workbook (version 2)

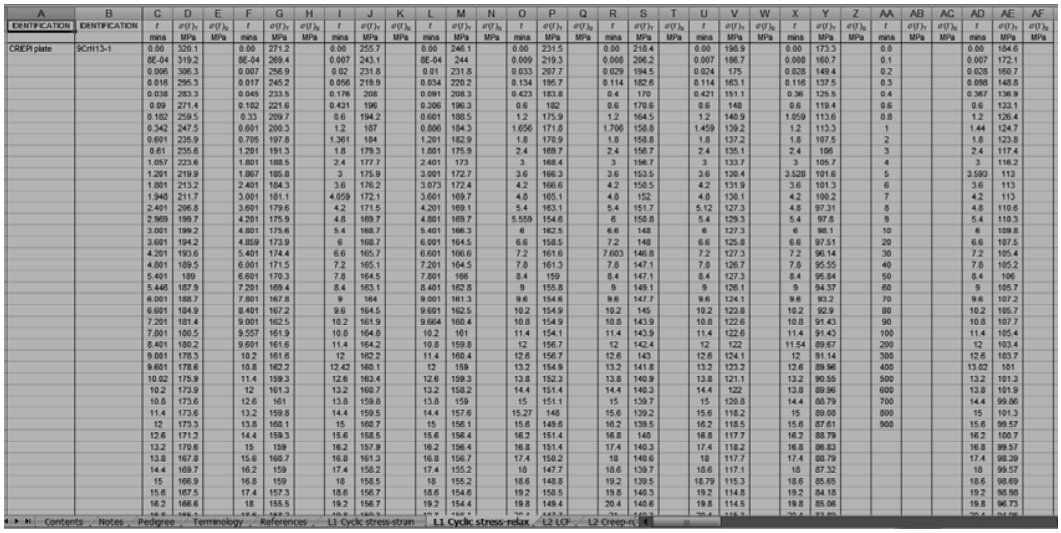

Figure A-4
Appearance of the L1 cyclic stress-relax sheet of the Creep-Fatigue Data Workbook (version 2)

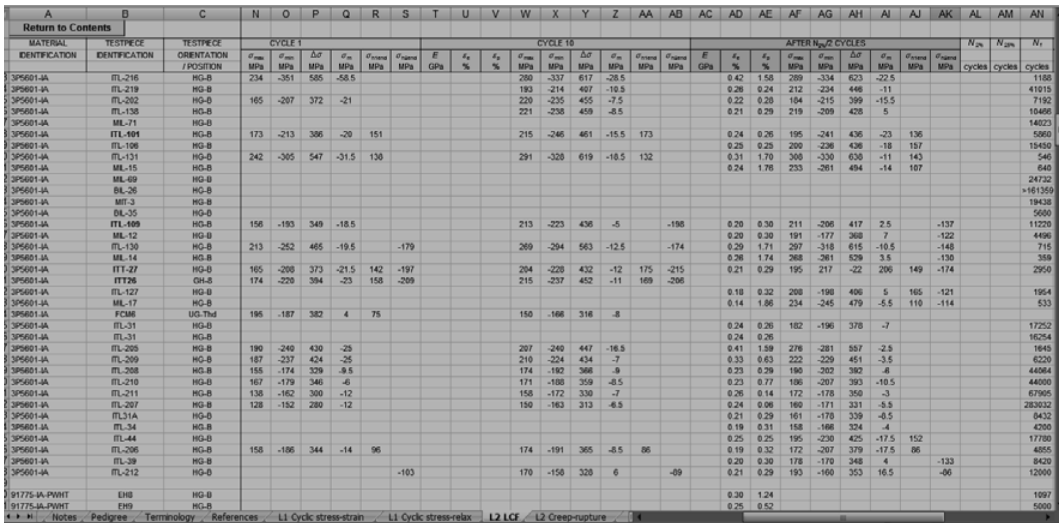

Figure A-5
Appearance of the L2 LCF sheet of the Creep-Fatigue Data Workbook (version 2)

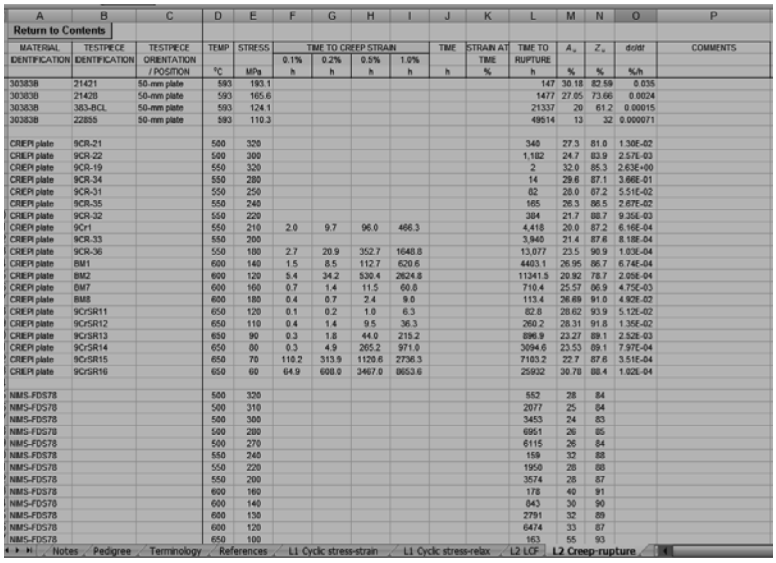

A	B	C	D	E	F	G	H	I	J	K	L	M	N	O	P
Return to Contents															
MATERIAL	TESTPIECE	TESTPIECE	TEMP	STRESS	TIME TO CREEP STRAIN				TIME	STRAIN AT	TIME TO	A_{re}	Z_{re}	do/dt	COMMENTS
IDENTIFICATION	IDENTIFICATION	ORIENTATION / POSITION			0.1%	0.2%	0.5%	1.0%		TIME	RUPTURE				
			°C	MPa	h	h	h	h	h	%	h	%	%	%/h	
30383B	21421	50-mm plate	593	193.1							147	30.18	82.59	0.035	
30383B	21428	50-mm plate	593	165.6							1477	27.65	73.66	0.0024	
30383B	383-BCL	50-mm plate	593	124.1							21337	20	61.2	0.00015	
30383B	22855	50-mm plate	593	110.3							49514	13	32	0.000071	
CREEP plate	9CR-21		500	320							340	27.3	81.0	1.30E-02	
CREEP plate	9CR-22		500	300							1,182	24.7	83.9	2.57E-03	
CREEP plate	9CR-19		550	320							2	32.0	85.3	2.63E+00	
CREEP plate	9CR-34		550	280							14	29.6	87.1	3.66E-01	
CREEP plate	9CR-31		550	250							62	28.0	87.2	5.51E-02	
CREEP plate	9CR-35		550	240							165	26.3	86.5	2.67E-02	
CREEP plate	9CR-32		550	220							384	21.7	88.7	9.35E-03	
CREEP plate	9Cr1		550	210	2.0	9.7	96.0	466.3			4,418	26.0	87.2	6.16E-04	
CREEP plate	9CR.33		550	200							3,940	21.4	87.6	8.18E-04	
CREEP plate	9CR-36		550	180	2.7	20.9	352.7	1648.8			13,077	23.5	90.9	1.03E-04	
CREEP plate	BM1		600	140	1.5	8.5	112.7	620.6			4403.1	26.95	86.7	6.74E-04	
CREEP plate	BM2		600	120	5.4	34.2	536.4	2624.8			11341.5	20.92	78.7	2.05E-04	
CREEP plate	BM7		600	160	0.7	1.4	11.5	60.8			710.4	25.57	86.9	4.75E-03	
CREEP plate	BM8		600	180	0.4	0.7	2.4	9.0			113.4	26.69	91.0	4.92E-02	
CREEP plate	9CrSR11		650	120	0.1	0.2	1.0	6.3			82.8	28.62	93.9	5.12E-02	
CREEP plate	9CrSR12		650	110	0.4	1.4	9.5	36.3			260.2	28.31	91.8	1.35E-02	
CREEP plate	9CrSR13		650	90	0.3	1.8	44.0	215.2			896.9	23.27	89.1	2.52E-03	
CREEP plate	9CrSR14		650	80	0.3	4.9	265.2	971.0			3094.6	23.53	89.1	7.97E-04	
CREEP plate	9CrSR15		650	70	110.2	313.9	1120.6	2736.3			7103.2	22.7	87.6	3.51E-04	
CREEP plate	9CrSR16		650	60	64.9	608.0	3467.0	8653.6			25932	30.78	88.4	1.62E-04	
NIMS-FDS78			500	320							552	28	84		
NIMS-FDS78			500	310							2077	25	84		
NIMS-FDS78			500	300							3453	24	83		
NIMS-FDS78			500	280							6951	26	85		
NIMS-FDS78			500	270							6115	26	84		
NIMS-FDS78			550	240							159	32	88		
NIMS-FDS78			550	220							1950	28	88		
NIMS-FDS78			550	200							3574	28	87		
NIMS-FDS78			600	160							178	40	91		
NIMS-FDS78			600	140							843	30	90		
NIMS-FDS78			600	130							2791	32	89		
NIMS-FDS78			600	120							6474	33	87		
NIMS-FDS78			650	100							163	55	93		

Notes | Pedigree | Terminology | References | L1 Cyclic stress-strain | L1 Cyclic stress-relax | L2 LCF | L2 Creep-rupture

Figure A-6
Appearance of the L2 creep-rupture sheet of the Creep-Fatigue Data Workbook (version 2)

B Nomenclature

A	tensile fracture elongation
A_R, A_R^*	creep-rupture elongation, predicted creep-rupture elongation
A_N	constant in Equation 3-3
$A_N(T)$	alternative Norton law constant when determined for single temperature
C_e, C_p	constants in Coffin-Manson Equation 4-5
d_C, d_C^*	creep damage fraction per cycle, PFD modified creep damage fraction per cycle (Equations 4-13 and 4-14)
d_C^P, d_C^S	creep damage due to primary (directly applied) loading, creep damage due to secondary (self-equilibrating) loading
$d_{C(t)}$, $d_{C(\varepsilon)}$	creep damage fraction per cycle (time fraction), creep damage fraction per cycle (strain fraction)
d_F, d_F^*	fatigue damage fraction per cycle, PCD modified fatigue damage fraction per cycle (Equation 4-8)
D_C, D_F	total creep damage fraction; total fatigue damage fraction
D'_F, D'_C	damage fraction coordinates defining intersection point in bilinear creep-fatigue damage summation diagram
E	elastic modulus
f	yield criterion
j	number of service-cycle types
k	thermal conductivity
K	hardening constant in Ramberg-Osgood model, Equation 3-1
LCF	low-cycle fatigue
n	creep-stress exponent (for example, in Equation 3-3)
N	number of cycles
N_i	number of cycles to crack initiation
PCD	prior creep deformed (damaged)
PFD	prior fatigue deformed (damaged)
Q_C	activation energy for creep
R	gas constant

R_m	ultimate tensile strength
$R_{p0.2}$	0.2% proof strength
$R_{R/t/T}$	creep-rupture strength for designated time and temperature
$R_{\varepsilon/t/T}$	creep strength for designated strain, time and temperature
t	time
t_h	duration of hold time or dwell period in a service cycle
t_R, t_R^*	observed time to creep-rupture, predicted time to creep-rupture
T	temperature
$T_{C/t}$	insignificant creep temperature (for a given time)
T_{max}, T_{min}	maximum and minimum temperature
T_{TRD}	TRD temperature (Equation 4-7)
TMF	thermo-mechanical fatigue
X	back stress tensor (Equation 3-2)
Z_R	reduction of area at creep rupture
α	coefficient of thermal expansion
β	hardening exponent in Ramberg-Osgood model, Equation 3-1
ε, $\Delta\varepsilon$	strain, strain range
ε_a	strain amplitude
ε_C,	creep strain
$\varepsilon_{C,min}$	minimum creep strain rate
$\varepsilon_{C,ave}$	average creep strain rate (that is, A_R/t_R)
ε_e, $\Delta\varepsilon_e$	elastic strain, elastic strain range
ε_p, $\Delta\varepsilon_p$	plastic strain, plastic strain range
$\Delta\varepsilon_t$	total strain range
γ_e, γ_p	exponents in Coffin-Manson Equation 4-5
σ, $\Delta\sigma$	stress, stress range
σ_a	stress amplitude
σ_{de}	stress at the end of the hold time (dwell period)
σ_{init}	initial stress (at start of hold time), often equal to σ_{max}

σ_{max}	maximum stress during cycle
σ_{min}	minimum stress during cycle
σ_o	limit of proportionality
σ_P	primary (directly applied) stress
σ_S	secondary (self-equilibrating) stress
σ_t	stress after time, *t* (for example, during strain-controlled hold time)
υ	frequency

Export Control Restrictions

Access to and use of EPRI Intellectual Property is granted with the specific understanding and requirement that responsibility for ensuring full compliance with all applicable U.S. and foreign export laws and regulations is being undertaken by you and your company. This includes an obligation to ensure that any individual receiving access hereunder who is not a U.S. citizen or permanent U.S. resident is permitted access under applicable U.S. and foreign export laws and regulations. In the event you are uncertain whether you or your company may lawfully obtain access to this EPRI Intellectual Property, you acknowledge that it is your obligation to consult with your company's legal counsel to determine whether this access is lawful. Although EPRI may make available on a case-by-case basis an informal assessment of the applicable U.S. export classification for specific EPRI Intellectual Property, you and your company acknowledge that this assessment is solely for informational purposes and not for reliance purposes. You and your company acknowledge that it is still the obligation of you and your company to make your own assessment of the applicable U.S. export classification and ensure compliance accordingly. You and your company understand and acknowledge your obligations to make a prompt report to EPRI and the appropriate authorities regarding any access to or use of EPRI Intellectual Property hereunder that may be in violation of applicable U.S. or foreign export laws or regulations.

The Electric Power Research Institute Inc., (EPRI, www.epri.com) conducts research and development relating to the generation, delivery and use of electricity for the benefit of the public. An independent, nonprofit organization, EPRI brings together its scientists and engineers as well as experts from academia and industry to help address challenges in electricity, including reliability, efficiency, health, safety and the environment. EPRI also provides technology, policy and economic analyses to drive long-range research and development planning, and supports research in emerging technologies. EPRI's members represent more than 90 percent of the electricity generated and delivered in the United States, and international participation extends to 40 countries. EPRI's principal offices and laboratories are located in Palo Alto, Calif.; Charlotte, N.C.; Knoxville, Tenn.; and Lenox, Mass.

Together...Shaping the Future of Electricity

Program:

Fossil Materials and Repair

1019778

Electric Power Research Institute
3420 Hillview Avenue, Palo Alto, California 94304-1338 • PO Box 10412, Palo Alto, California 94303-0813 USA
800.313.3774 • 650.855.2121 • askepri@epri.com • www.epri.com